Virtual photon emission in leptonic decays of charged pseudoscalar mesons

G. Gagliardi, F. Sanfilippo, and S. Simula

Istituto Nazionale di Fisica Nucleare, Sezione di Roma Tre, Via della Vasca Navale 84,
I-00146 Rome, Italy

V. Lubicz and F. Mazzetti

Dipartimento di Matematica e Fisica, Università Roma Tre and INFN,
Sezione di Roma Tre, Via della Vasca Navale 84, I-00146 Rome, Italy

G. Martinelli

Physics Department and INFN Sezione di Roma La Sapienza, Piazzale Aldo Moro 5, 00185 Roma, Italy

C. T. Sachrajda

Department of Physics and Astronomy, University of Southampton,
Southampton SO17 1BJ, United Kingdom

N. Tantalo

Dipartimento di Fisica and INFN, Università di Roma "Tor Vergata,"
Via della Ricerca Scientifica 1, I-00133 Roma, Italy

We study the radiative leptonic decays $P \to \ell \nu_\ell \ell'^+ \ell'^-$, where P is a pseudoscalar meson and ℓ and ℓ' are charged leptons. In such decays the emitted photon is off-shell and, in addition to the "point-like" contribution in which the virtual photon is emitted either from the lepton or the meson treated as a point-like particle, four structure-dependent (SD) form factors contribute to the amplitude. We present a strategy for the extraction of the SD form factors and implement it in an exploratory lattice computation of the decay rates for the four channels of kaon decays ($\ell, \ell' = e, \mu$). It is the SD form factors which describe the interaction between the virtual photon and the internal hadronic structure of the decaying meson, and in our procedure we separate the SD and point-like contributions to the amplitudes. We demonstrate that the form factors can be extracted with good precision and, in spite of the unphysical quark masses used in our simulation ($m_\pi \simeq 320$ MeV and $m_K \simeq 530$ MeV), the results for the decay rates are in reasonable semiquantitative agreement with experimental data (for the channels where these exist). Following this preparatory work, the emphasis of our future work will be on obtaining results at physical quark masses and on the control of the systematic uncertainties associated with discretization and finite-volume errors.

I. INTRODUCTION

The comparison of precise theoretical predictions for flavor-changing processes, in particular those which are suppressed in the Standard Model (SM), with experimental measurements is a fruitful approach to searches for new physics. For example, there have been experimental results suggesting the violation of lepton flavor universality which

is an important feature of the SM (see e.g., Refs. [1,2] and references therein). In order to confirm the presence of new physics and to elucidate its underlying structure it is important to study as many such processes as possible. In this paper we consider weak decays of the form $P \to \ell \nu_\ell \ell'^+ \ell'^-$, where ℓ and ℓ' are charged leptons, for which the decay rates start at $O(\alpha_{\rm em}^2)$.

For each decay $P \to \ell \nu_\ell \ell'^+ \ell'^-$, the computation of the decay rate requires the knowledge of four structure-dependent (SD) hadronic form factors, that depend on the invariant masses of the two leptonic pairs $\ell \nu_\ell$ and $\ell'^+ \ell'^-$ as well as of the leptonic decay constant f_P [see Eqs. (1)–(5) below]. The "point-like" (or inner-bremsstrahlung) contribution to the decay rate, in which the virtual photon is emitted

either from the lepton ℓ or from the meson P treated as a point-like particle, is readily calculable in perturbation theory, requiring only the well-known value of f_P as the nonperturbative input. The SD form factors describe the interaction between the virtual photon and the internal hadronic structure of the decaying meson and their computation in lattice quantum chromodynamics is the subject of this paper. This work is a natural extension of our detailed studies and computations of isospin-breaking corrections to leptonic decays [3–6] and to the calculation of leptonic radiative decays of the type $P \to \ell \nu_\ell \gamma$ where γ is a real photon [7,8].

Experimentally, only a few measurements exist. For the pion, the only measured decay rate is for the process $\pi^+ \to e^+ \nu_e e^+ e^-$, for which the Particle Data Group (PDG) reports a branching ratio of $(3.2 \pm 0.5) \times 10^{-9}$ [9]. For kaon decays measurements of the (partial) branching ratios have been performed by the E865 experiment at the Brookhaven National Laboratory AGS for the decays $K^+ \to e^+ \nu_e e^+ e^-$, $K^+ \to \mu^+ \nu_\mu e^+ e^-$ and $K^+ \to e^+ \nu_e \mu^+ \mu^-$ [10,11]. The branching ratios are found to be of $O(10^{-8})$. For decays with an $e^+ e^-$ pair in the final state a lower limit of about 150 MeV is imposed on the invariant mass of the lepton pair. Without such a cut the branching ratio would be dominated by the point-like contribution in the low $e^+ e^-$ invariant mass region which is of $O(10^{-5})$, so that the relevant SD contribution would not be detectable. For D mesons there are no data, while for B mesons there is an upper bound on $\mathrm{BR}(B^+ \to \mu^+ \nu_\mu \mu^+ \mu^-)$ of 1.6×10^{-8} [12].

In this paper we present the general strategy for the computation of the SD form factors and then implement the procedure in an exploratory lattice simulation for kaon decays, i.e., for $P = K$. The computation is performed using a single gauge ensemble of $N_f = 2 + 1 + 1$ flavors of twisted mass fermions generated by the European Twisted Mass Collaboration (ETMC) on a $32^3 \times 64$ lattice with lattice spacing $a = 0.0885$ fm and with unphysical light-quark masses such that the pion and kaon masses are $m_\pi \simeq 320$ MeV and $m_K \simeq 530$ MeV. Further details of the ensemble are given at the beginning of Sec. V. Our method enables us to determine each of the four SD form factors contributing to the amplitude with good precision, and to study their dependence on the kinematic variables. Using these form factors one can reconstruct separately all the contributions to the branching ratios: the point-like contribution, the SD one and that coming from the interference between the two. There has been one previous lattice study of these decays, in which a method was presented and implemented to compute the branching ratio for the decays $K \to \ell \nu_\ell \ell'^+ \ell'^-$ without separating the point-like contribution and determining the SD form factors themselves [13]. The exploratory computations in Ref. [13] were performed on a single gauge ensemble on a $24^3 \times 48$ lattice with $a \simeq 0.093$ fm and with

quark masses corresponding to $m_\pi \simeq 352$ MeV and $m_K \simeq 506$ MeV.[1]

In our computation and also that in Ref. [13], the kaon mass is smaller than twice the pion mass, $m_K < 2m_\pi$, so that there are no contributions of the form $K \to \pi\pi\ell\nu_\ell \to \ell\nu_\ell\gamma$, with an on-shell $\pi\pi\ell\nu_\ell$ intermediate state. With physical quark masses, contributions with such an intermediate state are present in the region of phase space in which $k^2 > 4m_\pi^2$, where k is the four-momentum of the virtual photon. This leads to finite-volume effects which decrease only as inverse powers of the volume and not exponentially [14–16]. This effect is particularly important for the decays of heavy mesons, where there are many more possible on-shell intermediate states. This issue, together with a complete study of all the systematic effects (due to discretization, finite volume and unphysical quark masses) will be the subject of our future studies.

For kaon decays, in addition to the lattice results from the computations reported here and in Ref. [13], theoretical information about the form factors comes from chiral perturbation theory (ChPT), which has been used at next-to-leading order (NLO) to estimate their values and their contribution to the branching ratios [17]. It is worth noting that at NLO in ChPT the form factors are constants, i.e., independent of the kinematical variables. In spite of the unphysical quark masses used in our simulation it has been interesting and instructive to compare our results with those from experiment (where available) and from NLO ChPT, as well as with those from Ref. [13]. Perhaps surprisingly, as can be seen from Tables IV–VII below, the results are generally in reasonable semiquantitative agreement but with some differences. In particular we speculate that the form factor H_1, defined in Eq. (5) may have to increase by $O(20\%)$ in order to get precise agreement with the experimental data (although there are also discrepancies in the experimental determination of H_1 from different decay channels). It will be important therefore, after this successful exploratory computation, to focus our future work on controlling and reducing the systematic uncertainties in order to obtain robust results at physical quark masses and in the continuum and infinite-volume limits. It will then be interesting to see whether the form factor H_1 will indeed change or whether there will be a different explanation for the differences between the experimentally observed rates and our current results.

For heavy mesons ChPT does not apply, and the one theoretical prediction was presented in Ref. [18] for B decays, where a vector meson dominance model has been used. The prediction for the $B^+ \to \mu^+ \nu_\mu \mu^+ \mu^-$ branching ratio of Ref. [18], however, is almost 4 times larger than the

---

[1]After the original version of this paper was posted on the arXiv, the authors of Ref. [13] updated their results. The values reported in Tables IV–VII below correspond to the updated results.

experimental upper limit obtained in Ref. [12]. It is therefore clear that a nonperturbative, model-independent lattice evaluation of the SD form factors is required.

The plan for the remainder of this paper is as follows. In Sec. II we define the hadronic tensor and the form factors into which it is decomposed. These are the main target of our lattice calculation. This is followed in Sec. III by an explanation of how the hadronic tensor can be determined from lattice computations and in Sec. IV by the presentation of our strategy for extracting the four SD form factors from the hadronic tensor. In Sec. V we present the details of the numerical computation of the SD form factors and in Sec. VI we use these form factors to compute (partially) integrated branching ratios for the four channels of kaon decays: $K^+ \to e^+ \nu_e \mu^+ \mu^-$, $K^+ \to \mu^+ \nu_\mu e^+ e^-$, $K^+ \to e^+ \nu_e e^+ e^-$ and $K^+ \to \mu^+ \nu_\mu \mu^+ \mu^-$. We also compare our results to the experimental measurements (where these exist) and to the predictions of ChPT. We present a summary and our conclusions in Sec. VII. There are two appendixes. In Appendix A we collect the formulas used to obtain the branching ratios from the form factors for the two channels in which $\ell \neq \ell'$. The corresponding formulas for the other two channels, i.e., when $\ell = \ell'$ are too lengthy to present here, but are available from the authors upon request. In Appendix B we discuss the nontrivial limit of the relevant lattice correlation function as the four-momentum of the photon, k, goes to zero, $k \to 0$. This is a key element in the subtraction of the point-like term from the hadronic matrix element, which itself is a necessary step to extract each of the SD form factors.

II. THE HADRONIC TENSOR IN MINKOWSKIAN AND EUCLIDEAN SPACE-TIME

At lowest order in the electroweak interaction, $P^+ \to l^+ \nu_l l'^+ l'^-$ decays are obtained from the diagrams depicted in Fig. 1. If $l = l'$, we also need to consider the diagrams obtained by interchanging the two identical charged leptons. The diagram in Figure 1(b) can readily be computed in perturbation theory, with the meson decay constant as the only required nonperturbative input. In Fig. 1(a) the

nonperturbative hadronic contribution to the matrix element factorizes, and is encoded in the following tensor:

$$H_W^{\mu\nu}(k, p) = \int d^4x \, e^{ik \cdot x} \langle 0|T[J_{\text{em}}^\mu(x) J_W^\nu(0)]|P(p)\rangle, \quad (1)$$

where $k = (E_\gamma, \boldsymbol{k})$ is the four-momentum of the virtual photon and $p = (E, \boldsymbol{p})$ is that of the incoming pseudoscalar meson P. The meson and photon energies satisfy $E = \sqrt{m_P^2 + \boldsymbol{p}^2}$ and $E_\gamma = \sqrt{k^2 + \boldsymbol{k}^2}$. The two operators

$$J_{\text{em}}^\mu(x) = \sum_f q_f \bar{\psi}_f(x) \gamma^\mu \psi_f(x)$$

$$J_W^\nu(x) = J_V^\nu(x) - J_A^\nu(x) = \bar{\psi}_D(x)(\gamma^\nu - \gamma^\nu \gamma_5) \psi_U(x), \quad (2)$$

are respectively the electromagnetic hadronic current and the hadronic weak current expressed in terms of the quark fields ψ_f having electric charge q_f in units of the charge of the positron; ψ_U and ψ_D indicate the fields of an up-type or a down-type quark. In Eq. (2) we have written the weak current, J_W^ν, corresponding to a positively charged meson P^+; for a negatively charged meson we make the replacement $D \leftrightarrow U$.

The hadronic tensor can be decomposed into form factors which are scalar functions encoding the nonperturbative strong dynamics. Following Ref. [19], we write

$$H_W^{\mu\nu} = H_{\text{pt}}^{\mu\nu} + H_{\text{SD}}^{\mu\nu}, \quad (3)$$

$$H_{\text{pt}}^{\mu\nu} = f_P \left[g^{\mu\nu} - \frac{(2p - k)^\mu (p - k)^\nu}{(p - k)^2 - m_P^2} \right], \quad (4)$$

$$H_{\text{SD}}^{\mu\nu} = \frac{H_1}{m_P}(k^2 g^{\mu\nu} - k^\mu k^\nu) + \frac{H_2}{m_P} \frac{[(k \cdot p - k^2)k^\mu - k^2(p - k)^\mu]}{(p - k)^2 - m_P^2}$$
$$\times (p - k)^\nu + \frac{F_A}{m_P}[(k \cdot p - k^2)g^{\mu\nu} - (p - k)^\mu k^\nu]$$
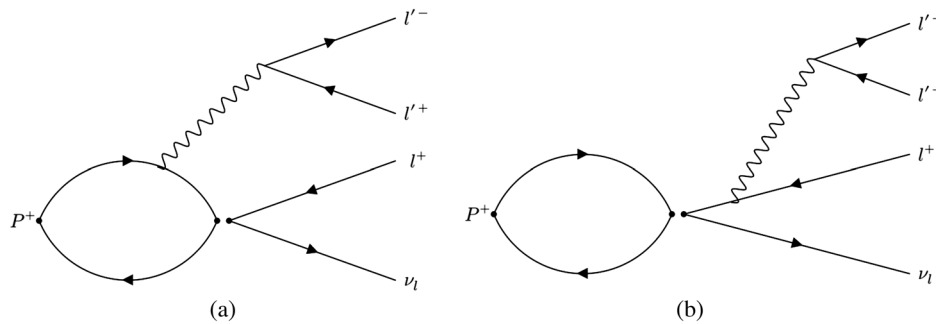$$- i \frac{F_V}{m_P} \epsilon^{\mu\nu\alpha\beta} k_\alpha p_\beta. \quad (5)$$

FIG. 1. Diagrams representing the virtual photon emission from the meson (a) and from the charged lepton (b), contributing to the process $P^+ \to l^+ \nu_l l'^+ l'^-$. We work in the electroquenched approximation in which the sea quarks are electrically neutral so contributions from disconnected diagrams are neglected (see Fig. 3 and the corresponding discussion).

With this decomposition we have separated the point-like contribution to the hadronic tensor from the structure-dependent one. The former depends only on the meson decay constant and is obtained by assuming a point-like meson. The SD contribution describes the interaction between the virtual photon and the hadronic structure of the pseudoscalar meson. The SD form factors, H_1, H_2, F_A and F_V, are scalar functions of k^2 and $(p-k)^2$. Note that, compared to our earlier work [see for example Eq. (B4) of Ref. [19] or Eq. (3) of Ref. [3]], we have modified the definitions of $H_{1,2}$ by a factor of m_P and introduced the denominator $(p-k)^2 - m_P^2$ in the factor multiplying H_2. In these earlier papers we were studying radiative corrections to leptonic decays with a real photon in the final state for which the form factors $H_{1,2}$ do not contribute. With the definitions in Eq. (5) all four form factors are now dimensionless and finite in the infrared limit. The main goal of this lattice study is to compute the SD form factors in order to reconstruct the full matrix element and subsequently the branching ratio for the decay. We do this in a way which separates the point-like contribution from that which depends on the hadronic structure.

In order to show how the hadronic tensor can be extracted from Euclidean correlation functions it is useful to express $H_W^{\mu\nu}(k,p)$ in terms of the contributions coming from the two different time orderings. By inserting a complete set of intermediate states we obtain the contributions from the two separate time orderings [$t_x < 0$ and $t_x > 0$, where $x = (t_x, \boldsymbol{x})$] as

$$H_W^{\mu\nu}(k,p) = H_{W,1}^{\mu\nu}(k,p) + H_{W,2}^{\mu\nu}(k,p), \tag{6}$$

where

$$H_{W,1}^{\mu\nu}(k,p) = -i \sum_{n_f : \boldsymbol{p}_{n_f}=\boldsymbol{p}-\boldsymbol{k}} \frac{\langle 0|J_W^\nu(0)|n_f\rangle\langle n_f|J_{\rm em}^\mu(0)|P(p)\rangle}{(E_\gamma + E_{n_f} - E)}, \tag{7}$$

$$H_{W,2}^{\mu\nu}(k,p) = -i \sum_{n : \boldsymbol{p}_n=\boldsymbol{k}} \frac{\langle 0|J_{\rm em}^\mu(0)|n\rangle\langle n|J_W^\nu(0)|P(p)\rangle}{(E_n - E_\gamma - i\epsilon)}, \tag{8}$$

and the sums over the intermediate states implicitly include the phase-space integration. The states $|n_f\rangle$ have the same flavor quantum numbers as the initial meson P, while the states $|n\rangle$ have zero additive flavor quantum numbers. For example, if we consider the decay of a K^+ and $J_W^\nu = \bar{s}\gamma^\nu(1-\gamma^5)u$, then the $|n_f\rangle$ have strangeness $S = -1$ and the $|n\rangle$ have $S = 0$.

Lattice correlation functions can only be computed in Euclidean space-time, and thus we have to translate the Minkowski Green function to the corresponding Euclidean one. By making the naive Wick rotation $t \to -it$ we obtain the Euclidean expression

$$H_E^{\mu\nu}(k,p) = -i \int d^4x\, e^{tE_\gamma - i\boldsymbol{k}\cdot\boldsymbol{x}} \langle 0|T[J_{\rm em}^\mu(x)J_W^\nu(0)]|P(p)\rangle. \tag{9}$$

As before, we insert a complete set of intermediate states and obtain contributions from each of the two time orderings:

$$H_E^{\mu\nu}(k,p) = H_{E,1}^{\mu\nu}(k,p) + H_{E,2}^{\mu\nu}(k,p), \tag{10}$$

$$H_{E,1}^{\mu\nu}(k,p) = -i \sum_{n_f : \boldsymbol{p}_{n_f}=\boldsymbol{p}-\boldsymbol{k}} \langle 0|J_W^\nu(0)|n_f\rangle\langle n_f|J_{\rm em}^\mu(0)|P(p)\rangle \int_{-\infty}^0 dt_x\, e^{t_x(E_\gamma + E_{n_f} - E)}, \tag{11}$$

$$H_{E,2}^{\mu\nu}(k,p) = -i \sum_{n : \boldsymbol{p}_n=\boldsymbol{k}} \langle 0|J_{\rm em}^\mu(0)|n\rangle\langle n|J_W^\nu(0)|P(p)\rangle \int_0^{+\infty} dt_x\, e^{-t_x(E_n - E_\gamma)}. \tag{12}$$

If the conditions

$$E_\gamma + E_{n_f} - E > 0, \tag{13}$$

$$E_n - E_\gamma > 0, \tag{14}$$

are satisfied, the time integrals converge and we have

$$H_E^{\mu\nu} = -i \sum_{n_f : \boldsymbol{p}_{n_f}=\boldsymbol{p}-\boldsymbol{k}} \frac{\langle 0|J_W^\nu(0)|n_f\rangle\langle n_f|J_{\rm em}^\mu(0)|P(p)\rangle}{E_\gamma + E_{n_f} - E} - i \sum_{n : \boldsymbol{p}_n=\boldsymbol{k}} \frac{\langle 0|J_{\rm em}^\mu(0)|n\rangle\langle n|J_W^\nu(0)|P(p)\rangle}{E_n - E_\gamma}. \tag{15}$$

If the inequalities (13) and (14) are satisfied then the Wick rotation leaves the hadronic tensor (1) unchanged, and thus the lattice calculation with Euclidean time can be done without particular difficulties. In such situations, the $i\epsilon$ in the second line of Eq. (8) is also unnecessary. On the other hand for external momenta such that the inequalities (13)–(14) are not satisfied the time integrals in Euclidean space-time diverge at large t_x. The above is a consequence of the analytic structure of the T product in Eq. (1): the presence of singularities (poles or cuts) in Minkowski space can prevent the possibility of making a naive Wick rotation. The presence of such singularities implies the existence of intermediate states with energies which are smaller than the external ones resulting in integrals over t_x which grow exponentially with the upper limit of integration. The conditions (13) and (14) correspond to the requirement that the internal states contributing to the correlation function all have energies larger than that of the external states (see Ref. [20] for more details).

In the above discussion we have not specified what the pseudoscalar meson P is but in this paper we apply the formalism to the decays of a kaon. For $t_x < 0$, i.e., when the electromagnetic current is inserted before the weak operator, the internal lightest state is given by a kaon with spatial momentum $\boldsymbol{p} - \boldsymbol{k}$, and it can be readily shown that the condition (13) is satisfied for every choice of the external momenta $\boldsymbol{p}$ and k. On the other hand, for $t_x > 0$, i.e., when the weak current is inserted before the electromagnetic one, the lowest-energy internal state is given by two pions with the same spatial momentum $\boldsymbol{k}$ as the virtual photon. Thus the condition (14) is satisfied only for $k^2 < 4m_\pi^2$ and for larger photon virtualities the correlator in Euclidean time is divergent. On a finite spatial lattice the spectrum of states $|n\rangle$ is discrete and so there is only a finite number of states with $k^2 > 4m_\pi^2$ and in practice the number of such states is small and the terms with the exponentially growing exponentials can be explicitly subtracted, thus extending the validity of the method beyond the region $k^2 < 4m_\pi^2$. The remaining issue is then the correction for the nonexponential finite-volume effects (analogous to those corrected by the Lellouch-Lüscher factor in $K \rightarrow \pi\pi$ decays [14]). We postpone a discussion of this issue to a future publication and for now we restrict our analysis, presented in Sec. V, to kaon decays with an unphysical pion mass such that $m_K < 2m_\pi$. Thus, two-pion internal states are always heavier than the external states and so conditions (13) and (14) are both satisfied.

Now that we have discussed the analytic continuation to Euclidean space-time, we proceed to the presentation of our strategy for extracting the SD form factors from suitable three-point lattice correlation functions.

III. THE HADRONIC TENSOR FROM LATTICE CORRELATION FUNCTIONS

The principal ingredient in evaluating the decay amplitude on a Euclidean lattice, with finite space-time volume $V = L^3 \times T$, is the correlation function

$$M_W^{\mu\nu}(t_x, t; \boldsymbol{k}, \boldsymbol{p}) = T\langle J_W^\nu(t)\hat{J}_{em}^\mu(t_x, \boldsymbol{k})\hat{P}(0, \boldsymbol{p})\rangle_{LT}, \quad (16)$$

where $\langle \ldots \rangle_{LT}$ denotes the average over the gauge field configurations at finite L and T. Note that in Eq. (16) we have placed the interpolating operator $\hat{P}(0, \boldsymbol{p})$ at time 0 and the weak current $J_W(t)$ at time t. The three operators in Eq. (16) are as follows:

(i) $\hat{P}(0, \boldsymbol{p})$ is the spatial Fourier transform of the interpolating operator for the decaying pseudoscalar meson at time $t = 0$:

$$\hat{P}(0, \boldsymbol{p}) = \sum_z e^{i\boldsymbol{p}\cdot\boldsymbol{z}} P(0, \boldsymbol{z}), \quad (17)$$

where $P(0, z) = i\bar{\psi}_U(0, \boldsymbol{z})\gamma_5\psi_D(0, \boldsymbol{z})$ for a positively charged meson or $P(0, z) = i\bar{\psi}_D(0, \boldsymbol{z})\gamma_5\psi_U(0, \boldsymbol{z})$ for a negatively charged one and $\psi_{U,D}$ indicate the fields of up-type and down-type quarks respectively. In this paper we study kaon decays so $U = u$ and $D = s$.

(ii) The renormalized hadronic weak current, $J_W^\nu(t) = J_V^\nu(t) - J_A^\nu(t)$ is placed at a generic time t and at the origin in space. The vector and axial currents, $J_V^\nu(t)$ and $J_A^\nu(t)$ respectively, satisfy the continuum Ward identities (up to discretization effects). In the twisted-mass discretization of the fermionic action [21], the vector and axial-vector currents we use are given by

$$J_V^\nu(t) = Z_A\bar{\psi}_D(t)\gamma^\nu\psi_U(t),$$
$$J_A^\nu(t) = Z_V\bar{\psi}_D(t)\gamma^\nu\gamma_5\psi_U(x), \quad (18)$$

for a positively charged meson or their Hermitian conjugates for a negatively charged one, where $Z_{A,V}$ are the renormalization factors ensuring that the Ward identities are satisfied.[2]

(iii) The electromagnetic current, $J_{em}^\mu(t_x, \boldsymbol{x})$, is defined by

$$J_{em}^\mu(t_x, \boldsymbol{x}) = \sum_f q_f J_f^\mu(t_x, \boldsymbol{x}), \quad (19)$$

where f is the flavor index and the charge q_f is equal to $2/3$ for up-type quarks and to $-1/3$ for down-type quarks. A possible choice for the lattice electromagnetic current is the local operator $J_f^\mu(t_x, \boldsymbol{x}) = Z_V^{loc}\bar{q}_f(t_x, \boldsymbol{x})\gamma^\mu q_f(t_x, \boldsymbol{x})$, where Z_V^{loc} is the finite renormalization constant of the vector current ($Z_V^{loc} = Z_A$ with twisted mass at maximal twist). We choose instead to use the exactly conserved lattice vector current which with twisted-mass Fermions at maximal twist is given by[3]

---

[2]Note that the renormalization factors to be used in twisted mass at maximal twist are chirally rotated with respect to those of standard Wilson fermions [22]. This is a consequence of the fact that the up-type and down-type quark fields in the action are discretized with opposite values of the Wilson parameter.

[3]With twisted boundary conditions we use the corresponding conserved current given by Eq. (B10) of Ref. [7].

$$J_f^\mu(x) = -\left\{\bar{\psi}_f(x)\frac{ir_f\gamma_5 - \gamma^\mu}{2}U_\mu(x)\psi_f(x+\hat{\mu}) - \bar{\psi}_f(x+\hat{\mu})\frac{ir_f\gamma_5 + \gamma^\mu}{2}U_\mu(x)^\dagger\psi_f(x)\right\}. \tag{20}$$

In Eq. (20), $U_\mu(x)$ are the QCD link variables and $r_f = \pm 1$ is the Wilson parameter of the flavor f [23]. The spatial momentum $\boldsymbol{k}$ of the current is assigned by defining

$$\hat{J}_{\text{em}}^\mu(t_x, \boldsymbol{k}) = \sum_{\boldsymbol{x}} e^{-i\boldsymbol{k}\cdot(\boldsymbol{x}+\hat{i}/2)} J_{\text{em}}^\mu(t_x, \boldsymbol{x}). \tag{21}$$

In order to obtain the decay amplitude, we need to integrate $M_W^{\mu\nu}(t_x, t; \boldsymbol{k}, \boldsymbol{p})$ over t_x, as seen for example in Eq. (1). To this end we construct the function

$$C_W^{\mu\nu}(t, E_\gamma, \boldsymbol{k}, \boldsymbol{p}) = -i\theta(T/2 - t)\sum_{t_x=0}^{T}(\theta(T/2 - t_x)e^{E_\gamma t_x} + \theta(t_x - T/2)e^{-E_\gamma(T-t_x)})M_W^{\mu\nu}(t_x, t; \boldsymbol{k}, \boldsymbol{p})$$

$$- i\theta(t - T/2)\sum_{t_x=0}^{T}(\theta(T/2 - t_x)e^{-E_\gamma t_x} + \theta(t_x - T/2)e^{-E_\gamma(t_x-T)})M_W^{\mu\nu}(t_x, t; \boldsymbol{k}, \boldsymbol{p}). \tag{22}$$

On a lattice with a large but finite temporal extent T, the required matrix element can be obtained from the first term in the top line of Eq. (22). This is illustrated in the left-hand diagram of Fig. 2 and it should be remembered that t_x can also be larger than t. The second term in the second line of Eq. (22) represents the time-reversed process (we discuss the properties of the matrix elements under time reversal at the end of this section) and is illustrated in the right-hand diagram of Fig. 2 and again it should be remembered that t_x can also be smaller than t. The second term in the top line of Eq. (22) represents, on a periodic lattice of finite temporal extent, the ordering where the electromagnetic current acts at an earlier time than the meson source that, in the reduction formula to create an initial meson state, should be asymptotically far in the past. Indeed, the contribution of this term disappears in the limit $T \to \infty$. On the lattices used here however, we have found that its inclusion corrects sizable finite T effects and improves the quality of the numerical fits of $C_W^{\mu\nu}(t, E_\gamma, \boldsymbol{k}, \boldsymbol{p})$. Similarly, the first term in the second line of Eq. (22) represents, for the time-reversed process, the electromagnetic currents acting at a

time larger than the meson source. Its contribution also disappears in the infinite-T limit, but its inclusion improves the quality of the fit of $C_W^{\mu\nu}(t, E_\gamma, \boldsymbol{k}, \boldsymbol{p})$.

Figure 3 contains two diagrams presented to illustrate two important points concerning our numerical calculation of the correlation functions and of the form factors. The diagram in the left panel shows a *quark-disconnected* contribution to the correlation function originating from the possibility that the virtual photon is emitted from sea quarks. In this paper we use the so-called electroquenched approximation in which the sea quarks are electrically neutral. In practice this means that we have neglected the contributions represented by the diagram in the left panel of Fig. 3. We note that the contribution of these diagrams vanishes in the limit of exact $SU(3)$ flavor symmetry.

The quark-connected diagram in the right panel of Fig. 3 is shown in order to explain the strategy we have used to set the values of the spatial momenta. We have exploited the fact that by working within the electroquenched approximation it is possible to choose arbitrary values of the spatial momenta by using different spatial boundary conditions for
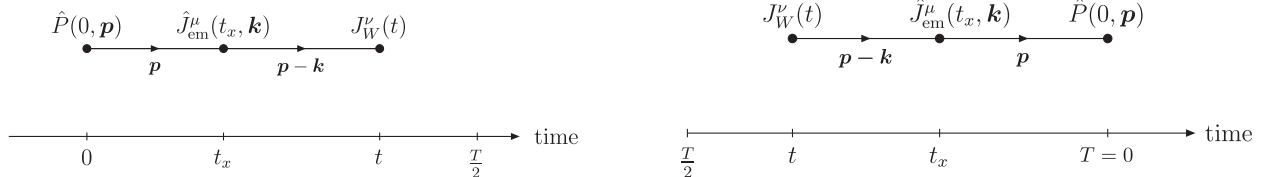

FIG. 2. Schematic diagrams representing the correlation function $C_W^{\mu\nu}(t, E_\gamma, \boldsymbol{k}, \boldsymbol{p})$ used to extract the form factors; see Eqs. (16) and (22). The interpolating operator for the meson $\hat{P}$ and the weak current J_W are placed at fixed times 0 and t and the electromagnetic current $\hat{J}_{\text{em}}$ is inserted at t_x which is integrated over $0 \le t_x \le T$, where T is the temporal extent of the lattice. The left and right panels correspond to the leading contributions to the correlation functions for $t < T/2$ and $t > T/2$ respectively, with mesons propagating with momenta $\boldsymbol{p}$ or $\boldsymbol{p} - \boldsymbol{k}$.
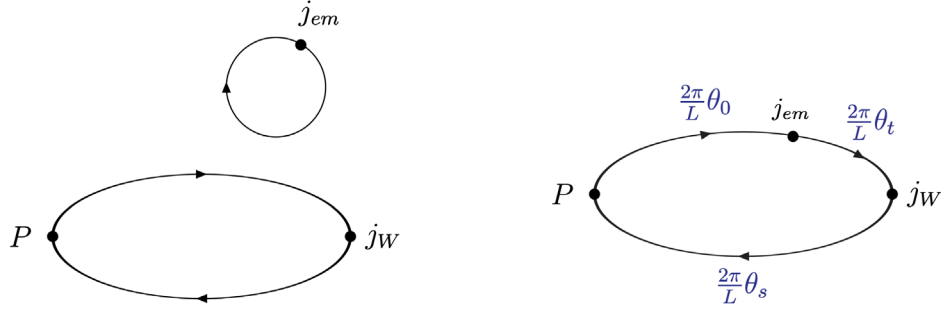
FIG. 3.   The diagram on the left represents the contributions to the correlation functions arising from the emission of the photon by the sea quarks. In our numerical simulations we work in the electroquenched approximation and neglect such diagrams. The diagram on the right explains our choice of the spatial boundary conditions, which allow us to set arbitrary values for the meson and photon spatial momenta. The spatial momenta of the valence quarks, modulo $2\pi/L$, in terms of the twisting angles are as indicated. Each diagram implicitly includes all orders in QCD.

the quark fields [24]. More precisely, we set the spatial boundary conditions for the "spectator" quark such that

$$\psi(x + \boldsymbol{n}L) = \exp(2\pi i \boldsymbol{n} \cdot \boldsymbol{\theta}_s)\psi(x), \qquad (23)$$

where $\boldsymbol{n}$ is a three-vector of integers and $\boldsymbol{\theta}_s$ is a three-vector of angles. For the temporal direction we employ antiperiodic boundary conditions. For each quark flavor f, we impose different boundary conditions on q_f and $\bar{q}_f$, the two component fields of J_f^μ. This is possible at the price of accepting violations of unitarity that are exponentially suppressed with the volume [25,26]. By setting the boundary conditions as illustrated in the figure we have thus

been able to choose arbitrary (nonquantized) values for the meson and photon spatial momenta

$$\boldsymbol{p} = \frac{2\pi}{L}(\boldsymbol{\theta}_0 - \boldsymbol{\theta}_s), \qquad \boldsymbol{k} = \frac{2\pi}{L}(\boldsymbol{\theta}_0 - \boldsymbol{\theta}_t), \qquad (24)$$

by tuning the real three-vectors $\boldsymbol{\theta}_{0,t,s}$. We find that the most precise results are obtained with small values of $|\boldsymbol{p}|$ and in particular with $\boldsymbol{p} = \boldsymbol{0}$.

In order to show that it is possible to extract the hadronic matrix element in Eq. (1) from the function in Eq. (22) we perform a spectral decomposition of $C_W^{\mu\nu}(t)$. On the assumption that the inequalities in Eqs. (13) and (14) are satisfied, we derive the relation

$$C_W^{\mu\nu}(t, E_\gamma, \boldsymbol{k}, \boldsymbol{p}) = \Theta(T/2 - t)\frac{e^{-t(E-E_\gamma)}\langle P|P|0\rangle}{2E}H_W^{\mu\nu}(\boldsymbol{k}, \boldsymbol{p}) + \Theta(t - T/2)\frac{e^{-(T-t)(E-E_\gamma)}\langle 0|P|P\rangle}{2E}[H_W^{\mu\nu}(\boldsymbol{k}, \boldsymbol{p})]^\dagger + \cdots \qquad (25)$$

where $H_W^{\mu\nu}(\boldsymbol{k}, \boldsymbol{p})$ is the *physical* matrix element defined in Eq. (1) and the dots represent the subleading exponentials, suppressed as $e^{-\Delta E t}$ or $e^{-\Delta E(T-t)}$, where ΔE can be either $E_n + E_\gamma - E$ or $E_n - E_\gamma$. We also see that when $t > T/2$ the correlator represents the time reversal of the original process. It is useful to note that, in order to separate the axial and vector form factors, it is enough to separately compute the correlation functions corresponding to the vector, $C_V^{\mu\nu}(t, E_\gamma, \boldsymbol{k}, \boldsymbol{p})$, and the axial, $C_A^{\mu\nu}(t, E_\gamma, \boldsymbol{k}, \boldsymbol{p})$, components of the weak current. Moreover, from the properties

$$[H_A^{\mu\nu}(k, p)]^\dagger = H_A^{\mu\nu}(k, p), \qquad [H_V^{\mu\nu}(k, p)]^\dagger = -H_V^{\mu\nu}(k, p) \qquad (26)$$

we deduce the following properties of the corresponding correlation functions under time reversal:

$$C_A^{\mu\nu}(T - t, T/2, E_\gamma, \boldsymbol{k}, \boldsymbol{p}) = C_A^{\mu\nu}(t, T/2, E_\gamma, \boldsymbol{k}, \boldsymbol{p}), \qquad C_V^{\mu\nu}(T - t, T/2, E_\gamma, \boldsymbol{k}, \boldsymbol{p}) = -C_V^{\mu\nu}(t, T/2, E_\gamma, \boldsymbol{k}, \boldsymbol{p}). \qquad (27)$$

We use these time reversal properties of the lattice correlators, to either symmetrize or antisymmetrize the correlators between the two halves $[0, T/2]$ and $[T/2, T]$ of the lattice and then we will work just within the first half of the lattice time extent, defining

$$H_L^{\mu\nu}(t, \boldsymbol{k}, \boldsymbol{p}) = \frac{2E}{e^{-t(E-E_\gamma)}\langle P|P|0\rangle}C_W^{\mu\nu}(t, E_\gamma, \boldsymbol{k}, \boldsymbol{p}) = H_W^{\mu\nu}(\boldsymbol{k}, \boldsymbol{p}) + \cdots \qquad (28)$$

where the subscript L stands for "lattice" and the ellipsis represents the subleading exponentials. In addition to decreasing the statistical error, averaging the correlation function between the two halves of the lattice in this way ensures $O(a)$ improvement, i.e., the reduction of the discretization errors to ones of $O(a^2)$.

In this section we have shown how to obtain the hadronic tensor from lattice correlation functions and we now proceed to discuss the extraction of all the structure-dependent hadronic form factors.

IV. EXTRACTION OF THE STRUCTURE-DEPENDENT FORM FACTORS

As already stated above, the axial and vector parts of the hadronic tensor can be evaluated separately in order to determine the corresponding form factors. In our numerical study we choose the meson to be at rest, $p = 0$ (the correlation functions are less noisy in this case) and the spatial momentum of the photon to be in the z direction, $k = (0, 0, k_z)$. The form factors depend on two independent variables which can be chosen to be the invariants k^2, where

k is the four-momentum of the photon, and $q^2 \equiv (p - k)^2$. In Sec. V we present our results in terms of the dimensionless variables x_k and x_q defined in Eq. (43) in terms of k^2 and q^2. In this section however, in which we discuss the extraction of the form factors from correlation functions computed in the frame defined above, it is more transparent to present the discussion with k^2 and k_z as the independent variables, together with the energy of the photon E_γ given by $E_\gamma^2 = k^2 + k_z^2$.

In the rest frame of the meson and with $k = (0, 0, k_z)$, the only nonzero elements of the vector component of the hadronic tensor, $H_V^{\mu\nu}$, are H_V^{12} and H_V^{21} which are related to the vector form factor F_V by

$$H_V^{12} = -H_V^{21} = iF_V k_z. \tag{29}$$

The axial component of the hadronic tensor, $H_A^{\mu\nu}$, is parametrized by the SD form factors F_A, H_1 and H_2, and by the meson decay constant f_P. In the reference frame defined above, the nonzero elements of $H_A^{\mu\nu}$ are given by

$$H_A^{00} = -H_1 \frac{k_z^2}{m_P} - H_2 \frac{k_z^2(m_P - E_\gamma)}{2m_P E_\gamma - k^2} - F_A \frac{k_z^2}{m_P} + f_P \frac{2m_P^2 - m_P E_\gamma + k_z^2}{2m_P E_\gamma - k^2}, \tag{30}$$

$$H_A^{03} = -H_1 \frac{E_\gamma k_z}{m_P} + H_2 \frac{k_z(E_\gamma^2 - k^2)}{2m_P E_\gamma - k^2} - F_A \frac{(m_P - E_\gamma)k_z}{m_P} - f_P \frac{k_z(2m_P - E_\gamma)}{2m_P E_\gamma - k^2}, \tag{31}$$

$$H_A^{30} = -H_1 \frac{E_\gamma k_z}{m_P} - H_2 \frac{k_z E_\gamma(m_P - E_\gamma)}{2m_P E_\gamma - k^2} + F_A \frac{k_z E_\gamma}{m_P} - f_P \frac{k_z(m_P - E_\gamma)}{2m_P E_\gamma - k^2}, \tag{32}$$

$$H_A^{33} = -H_1 \frac{E_\gamma^2}{m_P} + H_2 \frac{E_\gamma k_z^2}{2m_P E_\gamma - k^2} - F_A \frac{E_\gamma(m_P - E_\gamma)}{m_P} - f_P \frac{E_\gamma(2m_P - E_\gamma)}{2m_P E_\gamma - k^2}, \tag{33}$$

$$H_A^{11} = H_A^{22} = -H_1 \frac{k^2}{m_P} - F_A \frac{(m_P E_\gamma - k^2)}{m_P} - f_P. \tag{34}$$

Here and in the following we use continuum notation for the four-vectors but in lattice computations, in order to reduce the discretization uncertainties, the energy and momentum carried by the electromagnetic current should be understood by the following replacements:

$$k_z \to \hat{k}_z = \frac{2}{a}\sin\left(\frac{ak_z}{2}\right), \qquad E_\gamma = \frac{2}{a}\sinh^{-1}\left[\frac{a}{2}\sqrt{\hat{k}_z^2 + \left(\frac{2}{a}\sinh\left(\frac{a\sqrt{k^2}}{2}\right)\right)^2}\right] \tag{35}$$

where k_z and $\sqrt{k^2}$ are the continuum, physical values for the photon's spatial momentum (which here is directed along the z axis) and for the photon's virtuality respectively.

To determine the SD axial form factors from knowledge of the nonzero components of $H_A^{\mu\nu}$, it is necessary to subtract the point-like terms proportional to f_P. From the

previous equations, it follows that the point-like terms become dominant in the infrared limit, $k \to 0$, where the SD part of the hadronic tensor vanishes. This is expected, since soft photons cannot probe the internal structure of the meson. However, this poses the problem for the numerical evaluation of the SD form factors at small k^2, that $\mathcal{O}(a^2)$

discretization effects in the subtraction of the point-like contribution result in enhanced artifacts in the determined values of the SD form factors. Moreover, these artifacts diverge as $k \to 0$. This problem has already been encountered in our previous work on $P \to \ell\bar{\nu}_\ell\gamma$ decays [7], where it was found that performing the subtraction using the value of f_P extracted from two-point correlation functions results in unphysically large values of F_A in the soft-photon limit. In the same paper, we proposed a solution to this problem. We showed that by exploiting the electromagnetic Ward identity in the lattice theory, the subtraction of the point-like contribution can be performed nonperturbatively to all

orders in the lattice spacing, thus avoiding infrared-divergent lattice artifacts in the resulting SD form factors. In particular, we demonstrated that, for the diagonal spatial components of the lattice correlation function, which are smooth in the limit $k \to 0$, this can be achieved by using the values of f_P obtained from the same components evaluated at zero photon momentum [7].

A similar situation also occurs when the final-state photon is virtual, albeit in this case the lepton masses provide an energy-momentum cutoff for the photon. Proceeding in a similar way, we define the subtracted quantities for the diagonal components as follows:

$$\tilde{H}_A^{33}(k_z, k^2) \equiv H_A^{33}(k_z, k^2) - H_A^{33}(0,0)\frac{E_\gamma(2m_P - E_\gamma)}{2m_P E_\gamma - k^2} = -H_1\frac{E_\gamma^2}{m_P} + H_2\frac{E_\gamma k_z^2}{2m_P E_\gamma - k^2} - F_A\frac{E_\gamma(m_P - E_\gamma)}{m_P},$$

$$\tilde{H}_A^{11}(k_z, k^2) \equiv H_A^{11}(k_z, k^2) - H_A^{11}(0,0) = -H_1\frac{k^2}{m_P} - F_A\frac{(m_P E_\gamma - k^2)}{m_P}. \tag{36}$$

Unfortunately the same procedure cannot be used for the other components. The reason for this is that, in the limit $k \to 0$, the "excited" state consisting of a meson P with momentum $-\mathbf{k}$ and a photon with energy E_γ becomes degenerate with the "ground" state of the meson P at rest. In the $k \to 0$ limit, the off-diagonal components, C_A^{30} and C_A^{03} go to zero; the contribution of the $P + \gamma$ state cancels that of the ground state (we refer to Appendix B for a detailed discussion on this point). These components at zero photon momentum cannot therefore be used to subtract the contribution proportional to f_P. Instead we define a linear combination of the two off-diagonal components, which in the continuum cancels the point-like term proportional to f_P; that is

$$H_A^{[3,0]}(k_z, k^2) \equiv H_A^{30}(k_z, k^2) - H_A^{03}(k_z, k^2)\left(\frac{m_P - E_\gamma}{2m_P - E_\gamma}\right) = -H_1\frac{E_\gamma k_z}{2m_P - E_\gamma} - H_2\frac{k_z(m_P - E_\gamma)}{2m_P - E_\gamma} + F_A\frac{k_z m_P}{2m_P - E_\gamma}. \tag{37}$$

We have verified that the difference in Eq. (37) does not give rise to enhanced unphysical infrared effects from the residual discretization errors. In the present study of $K \to l\nu_l l'^+ l'^-$ decays, as mentioned above, we have an infrared cutoff on the photon virtuality k^2, given either by the non-negligible muon mass or by the experimental cut on the two-electron invariant mass $m_{ee} = \sqrt{k^2} > 145$ MeV [10]. Above these cutoffs we observe a smooth behavior of the form factors as a function of the photon's momentum without any anomalous increase in the infrared region.

An alternative possibility, one which we have not explored in this study, would have been to compute the correlation function with the meson in motion ($\mathbf{p} \neq \mathbf{0}$) and to use different components of the correlation functions to extract the form factors.

Once we compute three independent linear combinations of the three axial form factors using lattice QCD, the form factors themselves are obtained by inverting the matrix of coefficients. Specifically, our estimators of the axial form factors, $\bar{H}_1(t, k^2, k_z)$, $\bar{H}_2(t, k^2, k_z)$ and $\bar{F}_A(t, k^2, k_z)$, are obtained from the axial component of the lattice tensor $H_{L,A}^{\mu\nu}(t, k) \equiv H_{L,A}^{\mu\nu}(t, k, \mathbf{0})$ of Eq. (28) as follows:

$$\begin{pmatrix} \bar{H}_1(t, k^2, k_z) \\ \bar{H}_2(t, k^2, k_z) \\ \bar{F}_A(t, k^2, k_z) \end{pmatrix} \equiv Z(t) \begin{pmatrix} -\frac{E_\gamma k_z}{2m_P - E_\gamma} & -\frac{k_z(m_P - E_\gamma)}{2m_P - E_\gamma} & \frac{k_z m_P}{2m_P - E_\gamma} \\ -\frac{E_\gamma^2 + k^2}{m_P} & \frac{E_\gamma k_z^2}{2E_\gamma m_P - k^2} & \frac{E_\gamma^2 - 2E_\gamma m_P + k^2}{m_P} \\ \frac{k^2 - E_\gamma^2}{m_P} & \frac{E_\gamma k_z^2}{2E_\gamma m_P - k^2} & \frac{E_\gamma^2 - k^2}{m_P} \end{pmatrix}^{-1} \begin{pmatrix} H_{L,A}^{[3,0]}(t, k) \\ \tilde{H}_{L,A}^{33}(t, k) + \tilde{H}_{L,A}^{11}(t, k) \\ \tilde{H}_{L,A}^{33}(t, k) - \tilde{H}_{L,A}^{11}(t, k) \end{pmatrix} \tag{38}$$

where $Z(t)$ is the factor relating the matrix element of the bare local axial current, for a meson at rest, $f_P^{\text{bare}} m_P$, to the corresponding physical matrix element [up to terms of $O(a^2)$]. With twisted-mass fermions at maximal twist there is an exact partially conserved vector current relation which ensures that the physical decay constant can be obtained from two-point correlation functions of bare local pseudo-scalar operators [27,28]; this is denoted here by f_P^{2pt}. Thus

$$Z(t) = \frac{f_P^{\text{2pt}}}{f_P^{\text{bare}}} = \frac{-2 f_P^{\text{2pt}}}{(H_{L,A}^{11}(t,0) + H_{L,A}^{22}(t,0))} \qquad (39)$$

and at sufficiently large t, $Z(t)$ is independent of t. We recall that the diagonal components $\tilde{H}_{L,A}^{33}$ and $\tilde{H}_{L,A}^{11}$ are defined in Eq. (36) after the subtraction of the point-like contributions proportional to $H_{A,L}^{33}(t,0) = H_{A,L}^{11}(t,0) = H_{A,L}^{22}(t,0)$.

At large times $t/a \gg 1$ but with $t/a \ll T/2$, the estimators $\bar{H}_1(t, k^2, k_z)$, $\bar{H}_2(t, k^2, k_z)$ and $\bar{F}_A(t, k^2, k_z)$, tend to the corresponding form factors. In the limit $k_z \to 0$, two of the components of the vector on the right-hand side of Eq. (38), $H_{L,A}^{[3,0]}(t,k)$ and $\tilde{H}_{L,A}^{33}(t,k) - \tilde{H}_{L,A}^{11}(t,k)$, both go to zero for all values of k^2; see Eqs. (31)–(37). This fact can be used to define equivalent estimators of the form factors, obtained by making the following replacement(s) in Eq. (38):

$$H_{L,A}^{[3,0]}(t,k) \to H_{L,A}^{[3,0]}(t,k) - H_{L,A}^{[3,0]}(t,(\sqrt{k^2},\mathbf{0})) \qquad (40)$$

and/or

$$\begin{aligned} \tilde{H}_{L,A}^{33}(t,k) - \tilde{H}_{L,A}^{11}(t,k) &\to (\tilde{H}_{L,A}^{33}(t,k) \\ &- \tilde{H}_{L,A}^{33}(t,(\sqrt{k^2},\mathbf{0}))) - (\tilde{H}_{L,A}^{11}(t,k) - \tilde{H}_{L,A}^{11}(t,(\sqrt{k^2},\mathbf{0}))). \end{aligned} \qquad (41)$$

The correlated subtraction of the contribution coming from the kinematic point with the same value of k^2 but zero photon spatial momentum k_z, can reduce the statistical noise of the estimators and improve the corresponding plateaux and below we use this freedom to improve the resulting accuracy. The amount of improvement depends on the kinematic point and on the form factor being considered.

Finally, for the vector form factor F_V, we define the following estimator:

$$\bar{F}_V(t, k^2, k_z) = \frac{Z_A}{Z_V} Z(t) \frac{H_{L,V}^{12}(t,k) - H_{L,V}^{2,1}(t,k)}{2 i k_z}, \qquad (42)$$

which again for $t/a \gg 1$ and $t/a \ll T/2$ tends to F_V. The ratio of the axial (Z_A) and vector (Z_V) renormalization constants is needed to obtain the properly renormalized value of F_V when using twisted-mass fermions.

Having explained our procedure for extracting the SD form factors from three-point lattice correlation functions, we now proceed to presenting our numerical results.

V. NUMERICAL RESULTS FOR THE FORM FACTORS

In this section we implement the procedure developed in the preceding sections to study $K \to \ell \nu_\ell \ell'^+ \ell'^-$ decays numerically. The simulations have been performed on the A40.32 ensemble generated by the ETMC [3] with $N_f = 2 + 1 + 1$ dynamical quark flavors, a space-time volume of $32^3 \times 64$ and a lattice spacing of $a = 0.0885(36)$ fm. The analysis was performed on 100 gauge configurations. The light quarks are heavier than the corresponding physical ones and correspond to $m_\pi \simeq 320$ MeV and $m_K \simeq 530$ MeV. We used smeared interpolating sources for the kaon field, obtained applying 128 steps of Gaussian smearing with step-size parameter $\epsilon = 0.1$. Moreover, we used four stochastic sources on each time slice when inverting the Dirac operator. On this ensemble the values of the two renormalization constants are $Z_A = 0.731(8)$ and $Z_V = 0.587(4)$ [3]. The statistical analysis of the lattice data has been performed employing the jackknife resampling method in order to properly handle autocorrelation effects and cross correlations among the different form factors in the computation of the branching ratios.

Below we will compare our results for the form factors and branching ratios with those determined in experiment [10] and chiral perturbation theory. While these comparisons are interesting and instructive, it must be remembered that our computations were performed with unphysical quark masses, at a single value of the lattice spacing and on a single volume.[4] Until the corresponding systematic uncertainties are studied in the future, the comparison with the experimental measurements may be indicative, but cannot be considered definitive.

As already outlined in Sec. III, we used twisted boundary conditions in order to evaluate the hadronic tensor for a range of values of the photon's spatial momentum $\mathbf{k}$. To probe the region of the phase-space relevant for the four $K \to \ell \nu_\ell \ell'^+ \ell'^-$ decay channels, with ℓ, $\ell' = e, \mu$, we evaluate the Euclidean three-point functions $C^{\mu\nu}(t, E_\gamma, \mathbf{k}, \mathbf{p})$ for 15 different values of $(E_\gamma, \mathbf{k})$, with $\mathbf{k} = (0, 0, k_z)$, and restricte our analysis to the kaon rest frame $\mathbf{p} = 0$. We find it convenient to parametrize the phase space in terms of the two dimensionless parameters x_k and x_q, defined as

$$x_k \equiv \sqrt{\frac{k^2}{m_K^2}}, \qquad x_q \equiv \sqrt{\frac{q^2}{m_K^2}}, \qquad (43)$$

---

[4] We also compare our results with a previous lattice computation [13], which was performed on a $24^3 \times 48$ lattice with $a \simeq 0.093$ fm with quark masses corresponding to $m_\pi \simeq 352$ MeV and $m_K \simeq 506$ MeV.
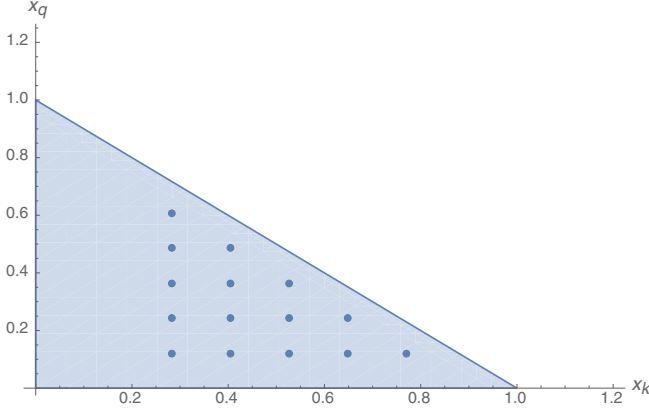
FIG. 4. The shaded area represents the range of allowed physical values of (x_k, x_q) when neglecting lepton masses, so that $0 < x_k < 1$ and $0 < x_q < 1 - x_k$. The points correspond to the 15 choices of (x_k, x_q) used in this analysis.

where q is the four-momentum of the lepton-neutrino pair created by the weak Hamiltonian. In terms of x_k and x_q the photon's four-momentum, $(E_\gamma, 0, 0, k_z)$ (in the kaon's rest frame), is given by

$$E_\gamma = \frac{m_K}{2}(1 + x_k^2 - x_q^2),$$
$$k_z = \frac{m_K}{2}\sqrt{(1 - x_k^2 - x_q^2)^2 - 4x_k^2 x_q^2}. \tag{44}$$

The range of values of x_k and x_q is given in terms of the lepton masses, m_ℓ and $m_{\ell'}$, by

$$\frac{m_\ell}{m_K} \le x_q \le 1 - x_k, \qquad \frac{2m_{\ell'}}{m_K} \le x_k \le 1 - \frac{m_\ell}{m_K}, \tag{45}$$

so that the phase space has a triangular shape in the x_k-x_q plane.

In Fig. 4 we show the positions of the 15 simulated kinematic configurations, which we take as equally spaced in the x_k-x_q plane. For completeness, the corresponding numerical values of x_k and x_q are reported in Table I. It should be noted that our computations are limited to $x_k \ge 0.28$. This choice is appropriate to describe both the cases in which a $\mu^+\mu^-$ or a e^+e^- pair is produced in the radiative decay of the kaon. Indeed, in the first case the lowest allowed value of x_k is given by $2m_\mu/m_K \simeq 0.428$, while for decays in which an e^+e^- pair is produced, although very low values of x_k are kinematically allowed, the experimental branching ratios have been determined

with values of the electron-positron invariant mass $\sqrt{k^2} > 145$ MeV ($x_k > 0.294$) for $K^+ \to \mu^+\nu_\mu e^+e^-$ decays and $\sqrt{k^2} > 150$ MeV ($x_k > 0.304$) for $K^+ \to e^+\nu_e e^+e^-$ decays [10].

In Figs. 5–7, we present the estimators $\bar{H}_1(t, x_k, x_q)$, $\bar{H}_2(t, x_k, x_q)$, $\bar{F}_A(t, x_k, x_q)$ and $\bar{F}_V(t, x_k, x_q)$ for selected values of x_k and x_q. In each figure, the shaded region indicates the result of a constant fit in the corresponding time interval. Figures 5 and 6 illustrate the feature that for kinematics corresponding to small values of k_z (i.e., when $x_q + x_k \simeq 1$) the estimator of the axial form factor F_A becomes somewhat noisy leading to increased uncertainties in its determination. On the other hand, for other values of (x_k, x_q) and for all other form factors, the precision achieved is very good and typically of the order of 5–10%. To check the stability of our numerical results, we verified that the values of the form factors remain consistent within errors by changing the time interval adopted for the fits by a few units.

In order to evaluate the decay rate, we fit the lattice form factors, using two different *Ansätze* to describe their dependence on x_k and x_q. The first is a simple polynomial in x_k^2 and x_q^2 given by

$$F_{\text{poly}}(x_k, x_q) = a_0 + a_k x_k^2 + a_q x_q^2, \tag{46}$$

where a_0, a_k and a_q are free fitting parameters. We find that this simple form represents our data very well and the corresponding results presented below are obtained using Eq. (46). However, we have also performed fits using *Ansätze* which include additional terms which are quartic in x_k and x_q, i.e., terms proportional to $x_k^2 x_q^2$, x_k^4 and x_q^4. We find that including all or some of such terms does not improve the fits, generally results in an overfit of our data and only negligibly changes the results for the form factors and decay rates. This is not surprising as the 15 points in the (x_k, x_q) plane at which we compute the form factors (see Table I) cover well the kinematic regions studied in the E865 experiment [10,11] to which we compare our results in Sec. VI. We therefore require only minor interpolations of our results to be able to perform the phase-space integrations.

The second *Ansatz* has a pole-like structure of the form

$$F_{\text{pole}}(x_k, x_q) = \frac{A}{(1 - R_k x_k^2)(1 - R_q x_q^2)}, \tag{47}$$

TABLE I. Table of the values of x_k and x_q corresponding to the 15 simulated kinematic points.

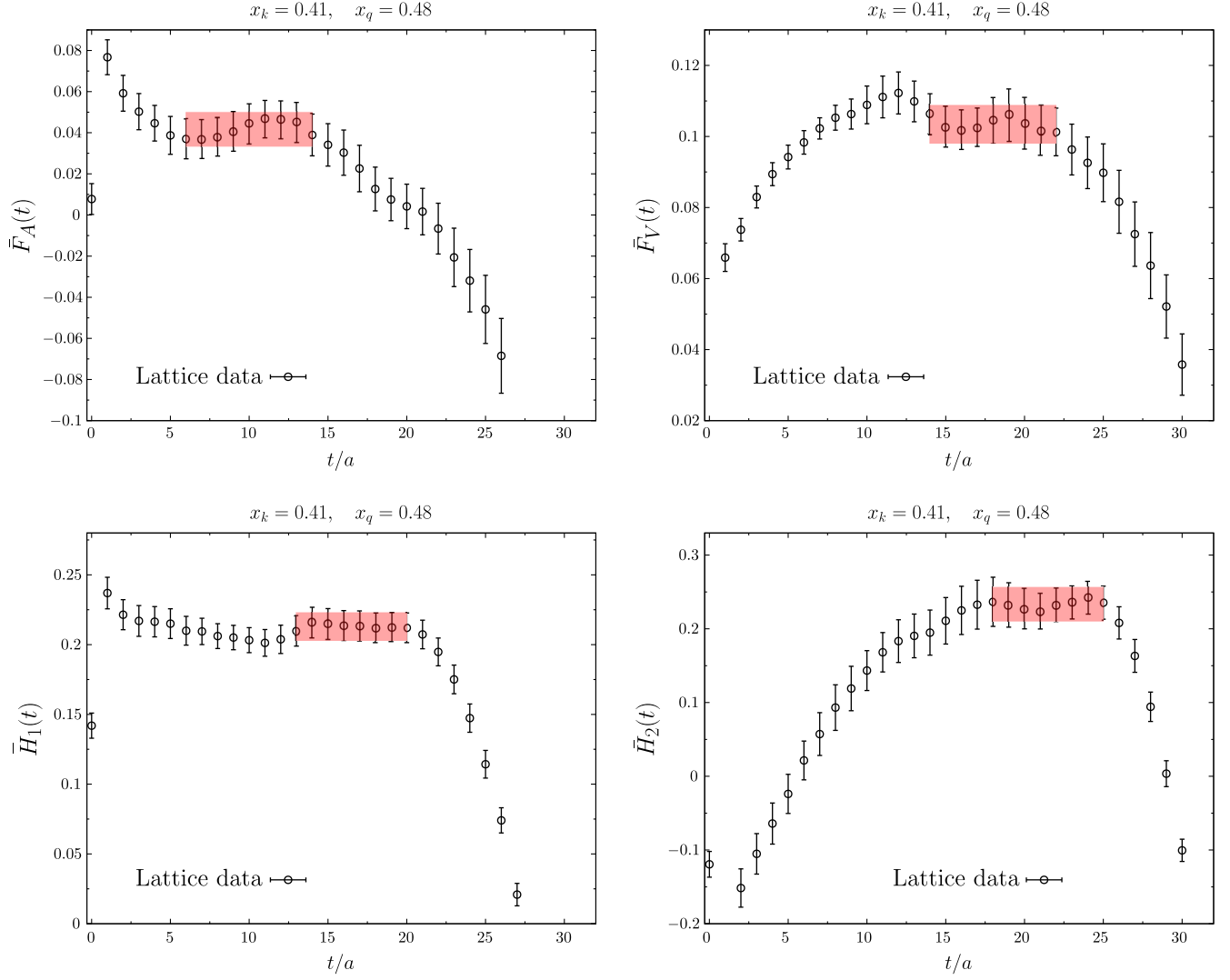| Kinematics	1	2	3	4	5	6	7	8	9	10	11	12	13	14	15
x_k	0.28	0.28	0.28	0.28	0.28	0.41	0.41	0.41	0.41	0.53	0.53	0.53	0.65	0.65	0.77
x_q	0.12	0.24	0.36	0.48	0.61	0.12	0.24	0.36	0.48	0.12	0.24	0.36	0.12	0.24	0.12

FIG. 5.   Extraction of the form factors F_A, F_V, H_1, H_2 from the plateaux of the corresponding estimator. The data correspond to $x_k = 0.41$ and $x_q = 0.48$.

where again A, R_k and R_q are free fitting parameters. The resulting fitting curves, along with the lattice data and with the ChPT prediction, are shown, for all four form factors H_1, H_2, F_A and F_V, in the panels of Figs. 8 and 9, as a function of x_q at fixed x_k, and vice versa. The quality of the fit in all cases is very good, with the reduced χ^2 always smaller than one. The parameters of both the polynomial and pole-like fits are collected in Table II.

The one-loop ChPT predictions for the form factors H_1, H_2, F_A and F_V of the K^+ meson read [17]

$$F_V = \frac{m_K}{4\sqrt{2}\pi^2 F}, \qquad F_A = \frac{4\sqrt{2}m_K}{F}(L_9^r + L_{10}^r),$$

$$H_1(k^2) = 2f_K m_K \frac{(F_V^K(k^2) - 1)}{k^2},$$

$$H_2(k^2) = 2f_K m_K \frac{(F_V^K(k^2) - 1)}{k^2}, \qquad (48)$$

where F is the ChPT leading-order low-energy constant (LEC), while L_9^r and L_{10}^r are ChPT LECs at next-to-leading order. The one-loop ChPT prediction for the kaon electromagnetic form factor $F_V^K(k^2)$ (which depends on F and L_9^r) can be found in Ref. [17]. In the following we will evaluate the ChPT predictions for the form factors using the physical charged kaon and pion masses and setting either $F = f_\pi/\sqrt{2}$ or $F = f_K/\sqrt{2}$, where f_π and f_K are the physical values of these decays constants. We label these two determinations as ChPT(f_π) and ChPT(f_K), respectively. For the LECs L_9^r and L_{10}^r, we use the values

$$L_9^r = 6.9 \times 10^{-3}, \qquad L_{10}^r = -5.2 \times 10^{-3}, \quad (49)$$

taken from Ref. [29]. Notice that at this order, the one-loop prediction for the form factors does not depend on q^2. Moreover, the dependence on the virtuality k^2 is very mild as well, and only enters the prediction for the form factors
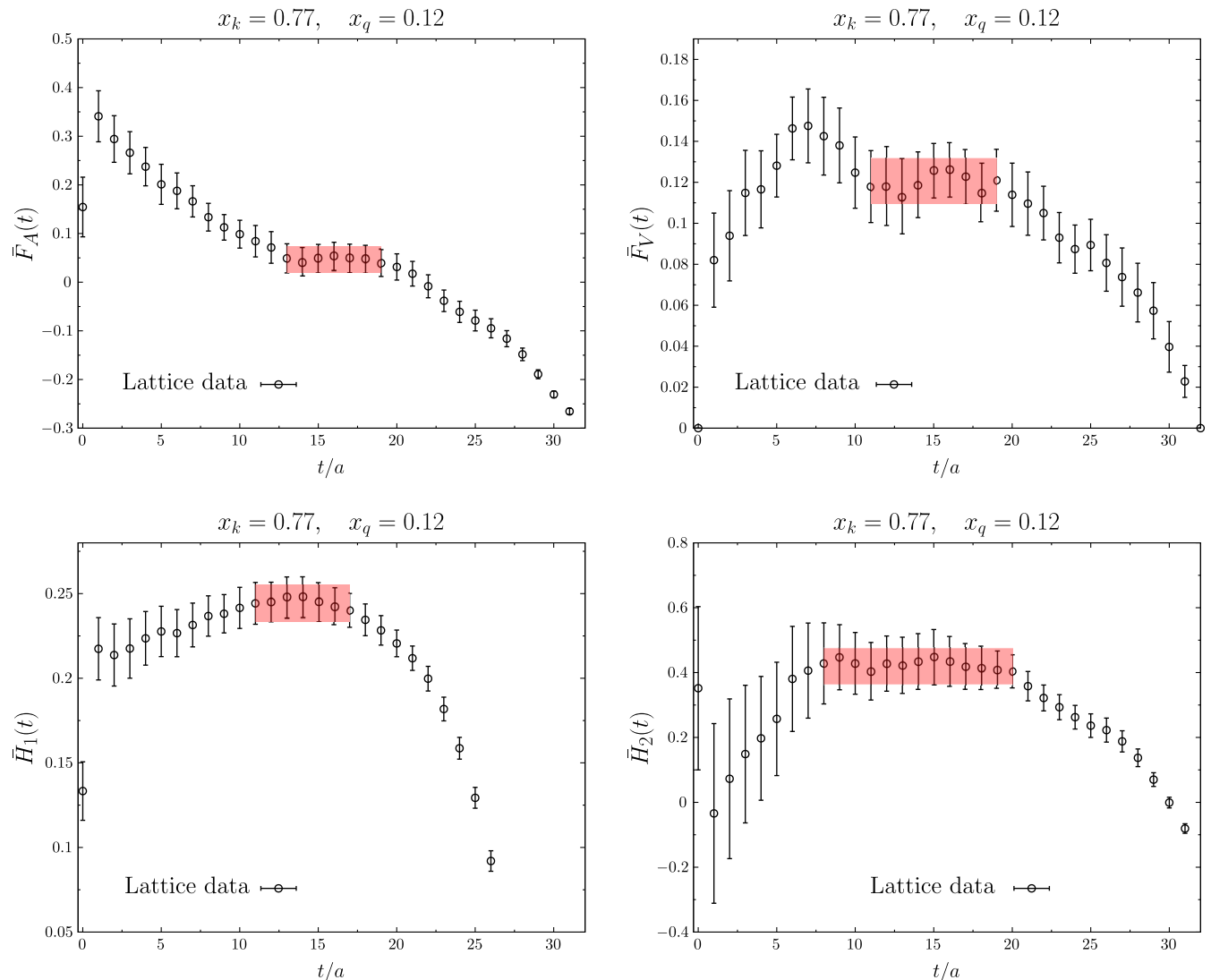
FIG. 6. Extraction of the form factors F_A, F_V, H_1, H_2 from the plateaux of the corresponding estimator. The data correspond to $x_k = 0.77$ and $x_q = 0.12$.

H_1 and H_2, through the higher-order corrections to the linear parametrization for the electromagnetic form factor

$$F_V^K(k^2) = 1 + \frac{\langle r_K^2 \rangle}{6} k^2 + \mathcal{O}(k^4), \qquad (50)$$

where $\langle r_K^2 \rangle$ is the kaon's mean-square radius. From the figures it can be seen that our results are reasonably consistent with the ChPT prediction. However, note that, at NLO, ChPT does not include any momentum dependence of the form factors and so the comparison should be made with their values at $x_k = 0$ and $x_q = 0$, that is with the parameters a_0 or A. Moreover, even at zero momentum transfer, on the one hand we do not expect the NLO ChPT

prediction to be exact, while on the other hand our lattice estimates are affected by systematic errors, such as the continuum, chiral and infinite-volume extrapolations, that will be studied in the future.

In Ref. [10], a vector-meson dominance (VMD) *Ansatz* was used in order to describe the momentum behavior of the form factors H_1, F_A, F_V, and was then used in order to reproduce the experimental data.[5] Within the VMD framework, the momentum dependence of the form factors is assumed to be determined by the masses of the low-lying resonances created by the electromagnetic and weak

---

[5]The authors of Ref. [10] assumed that H_2 only contributes through the kaon's electromagnetic form factor and neglected the other unknown SD contributions. These however, are suppressed in ChPT [17].
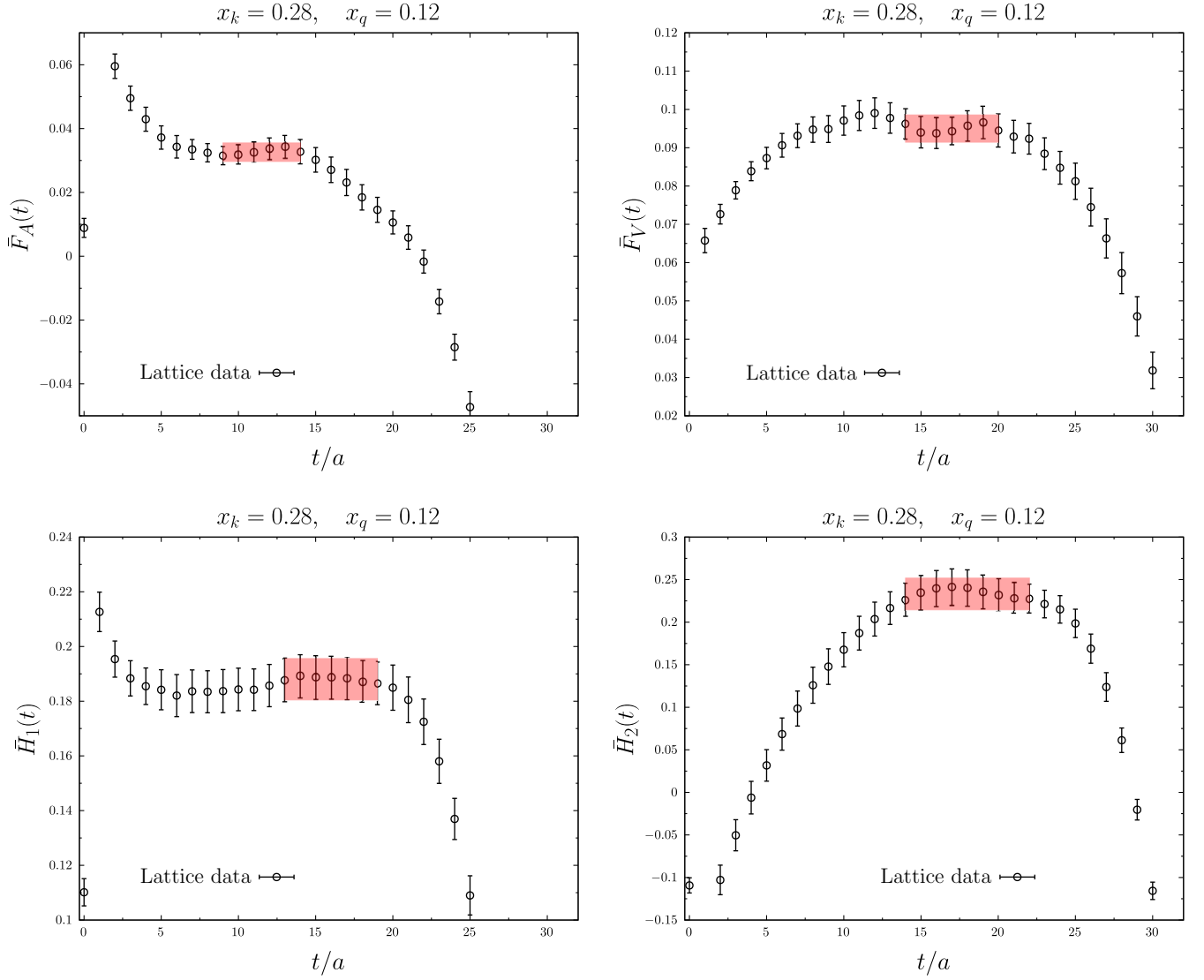
FIG. 7. Extraction of the form factors F_A, F_V, H_1, H_2 from the plateaux of the corresponding estimator. The data correspond to $x_k = 0.28$ and $x_q = 0.12$.

currents. In Ref. [10], for each of the three form factors, the fitting function has been taken to be of the form

$$F_{\text{VMD}}(x_k, x_q) = \frac{F(0,0)}{(1 - x_k^2 m_K^2/m_\rho^2)(1 - x_q^2 m_K^2/m_{K^*}^2)}, \quad (51)$$

where $F(0,0)$ is the only free fitting parameter. In Eq. (51), m_ρ is the mass of the ρ meson, while m_{K^*} is the mass of the $K^*(1270)$ in the axial channel, and that of the $K^*(892)$ in the vector one. Thus, the VMD model corresponds to fixing, in the pole-like fit of Eq. (47), $R_k = (m_K/m_\rho)^2 \simeq 0.4116$, and $R_q = (m_K/m_{K^*}(1270))^2 \simeq 0.1513$ for the axial channel and $R_q = (m_K/m_{K^*}(892))^2 \simeq 0.3064$ for the vector one.

In Table III, we compare the values of $F(0,0)$ obtained from experiment assuming VMD and presented in Ref. [10], with the corresponding values of the form factors at zero x_k and x_q that we obtained from our lattice data using the pole fit of Eq. (47), i.e., the values for the parameter A reported in Table II. In Fig. 10 we compare our lattice data for the form factors H_1, F_A, F_V, with the result of the experimental VMD fits performed in Ref. [10]. Despite the systematic uncertainties affecting our lattice computation, the results are in reasonably good agreement. The largest discrepancy that we observe, which is of $\mathcal{O}(20\%)$, is for the form factor H_1.

We also notice that the fitted values of R_k and R_q reported in Table II, are in qualitative agreement with the
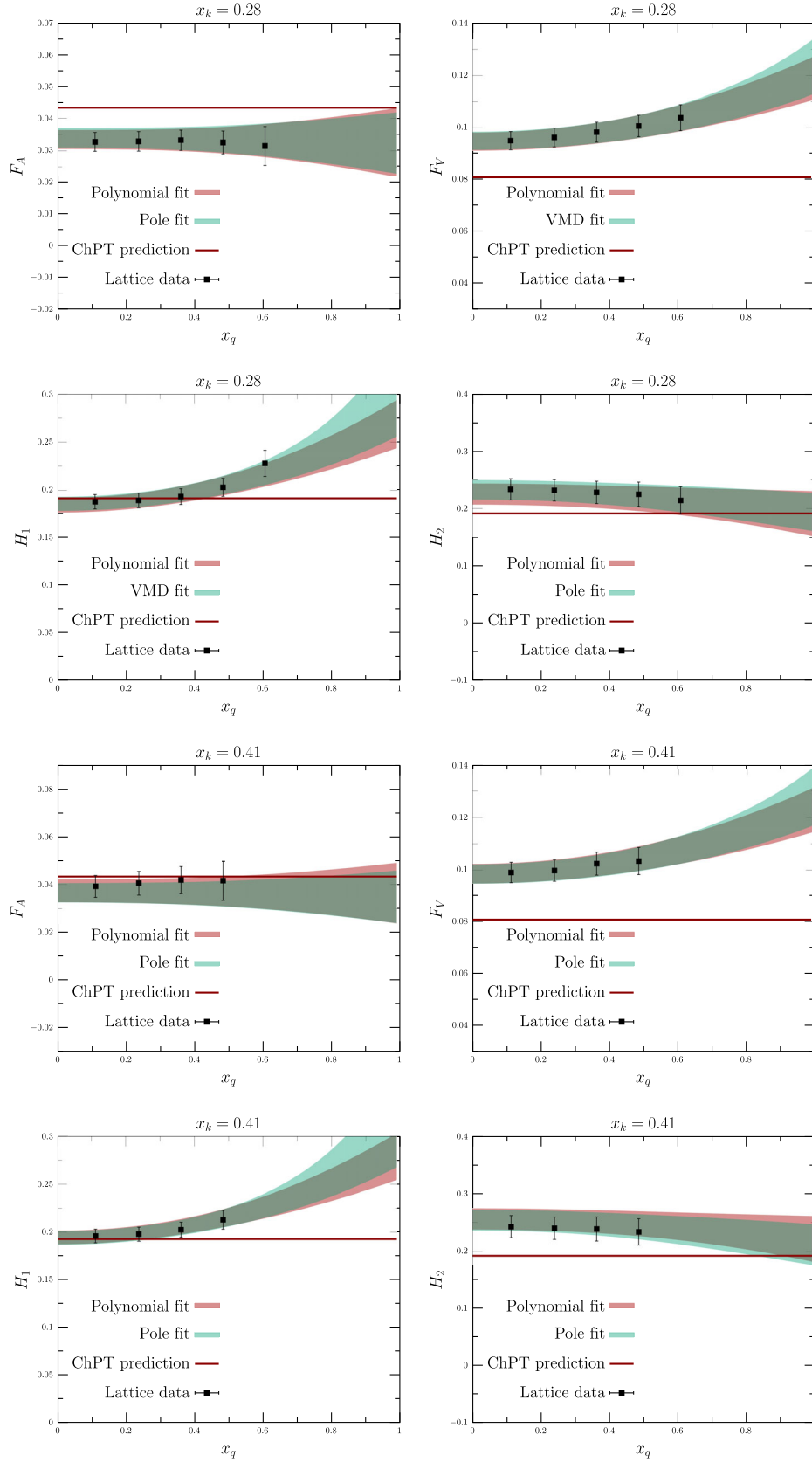
FIG. 8. The fitting functions corresponding to the polynomial and the pole-like fits of Eqs. (46) and (47) are plotted, along with the lattice data, as functions of x_q and at a fixed value of $x_k = 0.28$ (panels 1–4) and $x_k = 0.41$ (panels 5–8). The red line corresponds to the one-loop ChPT prediction with $F = f_K/\sqrt{2}$.
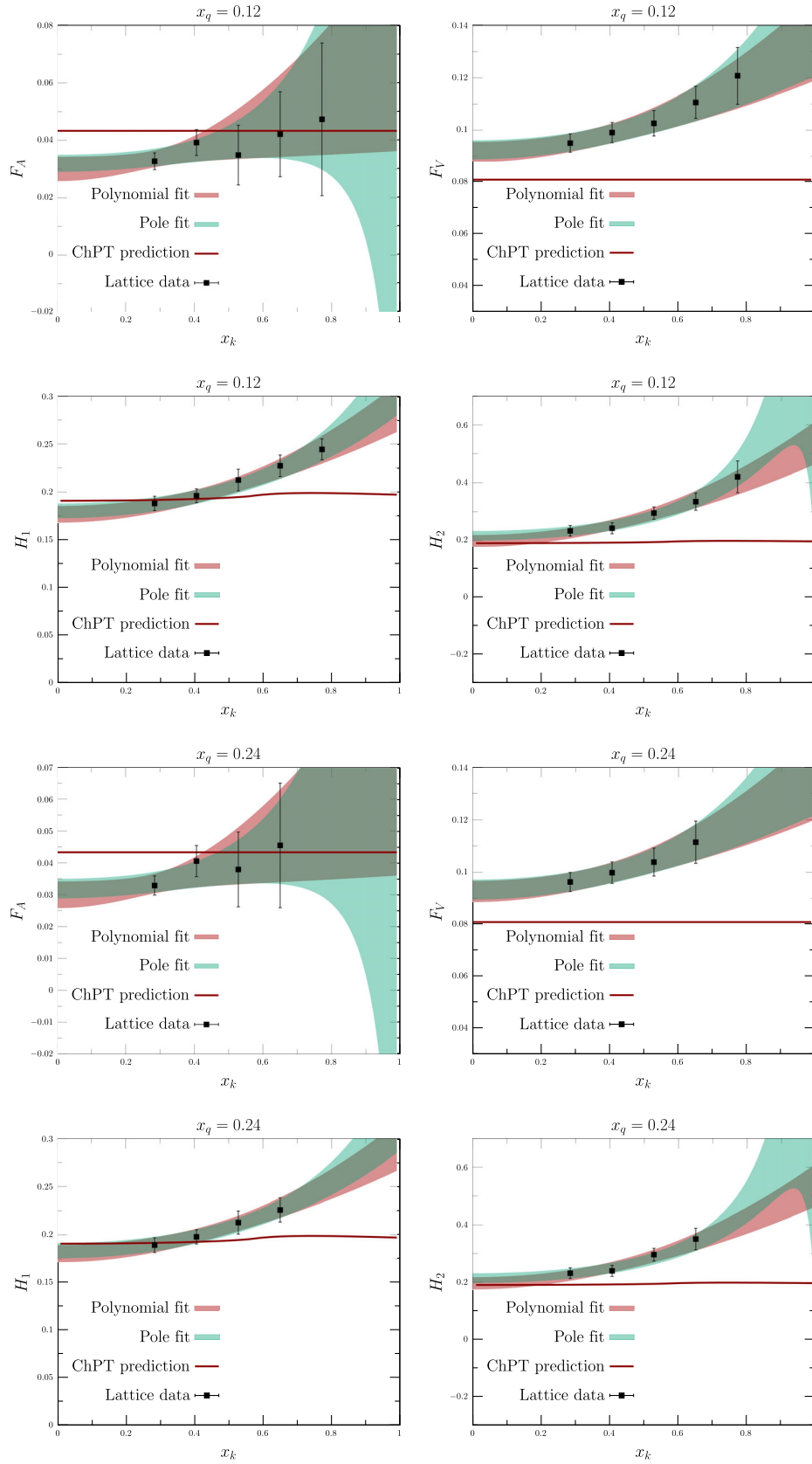
FIG. 9.   The fitting functions corresponding to the polynomial and the pole-like fits of Eqs. (46) and (47) are plotted, along with the lattice data, as functions of x_k and at a fixed value of $x_q = 0.12$ (panels 1–4) and $x_q = 0.24$ (panels 5–8). The red line corresponds to the one-loop ChPT prediction with $F = f_K/\sqrt{2}$.

TABLE II. Values of the fit parameters for all the form factors, as obtained from the polynomial and pole-like fits of Eqs. (46) and (47). In Appendix C we report the correlation matrix among the fit parameters, for each of the two *Ansätze*.

	a_0	a_k	a_q	A	R_k	R_q
H_1	0.1755(88)	0.113(30)	0.086(24)	0.1792(78)	0.453(88)	0.40(10)
H_2	0.199(21)	0.341(84)	−0.03(3)	0.217(17)	0.87(12)	−0.2(2)
F_A	0.0300(43)	0.04(4)	0.00(1)	0.0320(30)	0.74(50)	0.0(3)
F_V	0.0912(39)	0.044(18)	0.0246(59)	0.0921(38)	0.38(13)	0.233(49)

TABLE III. Comparison of the values of the VMD fit parameters $F(0,0)$ for the form factors H_1, F_A and F_V as obtained in Ref. [10] with the lattice results from this work [using the pole fit in Eq. (47)].

	$H_1(0,0)$	$F_A(0,0)$	$F_V(0,0)$
This work	0.1792(78)	0.0320(30)	0.0921(38)
Experiment [10]	0.227(19)	0.035(19)	0.112(18)

values predicted by VMD, albeit with large errors. In particular we are not able to see a clear x_k and x_q dependence in the lattice data for F_A, while the value of

the fit parameter R_q, for the form factor H_1, seems to be larger than the expectation based on VMD. Concerning the form factor H_2, the dominant contribution from the low-lying intermediate states comes from the virtual K^+ state created by the weak current [$|n_f\rangle = |K^+\rangle$ in Eq. (7)]. The resulting contribution $H_{2;K^+}$ to H_2 is then proportional to the electromagnetic kaon form factor $F_V^K(x_k)$ [17]

$$H_{2;K^+} = \frac{2f_K}{m_K} \frac{F_V^K(x_k) - 1}{x_k^2}, \tag{52}$$

in agreement with the prediction from ChPT presented in Eq. (48). As shown in Table II and in Fig. 8, we do not see any clear x_q dependence in our lattice data for H_2 in
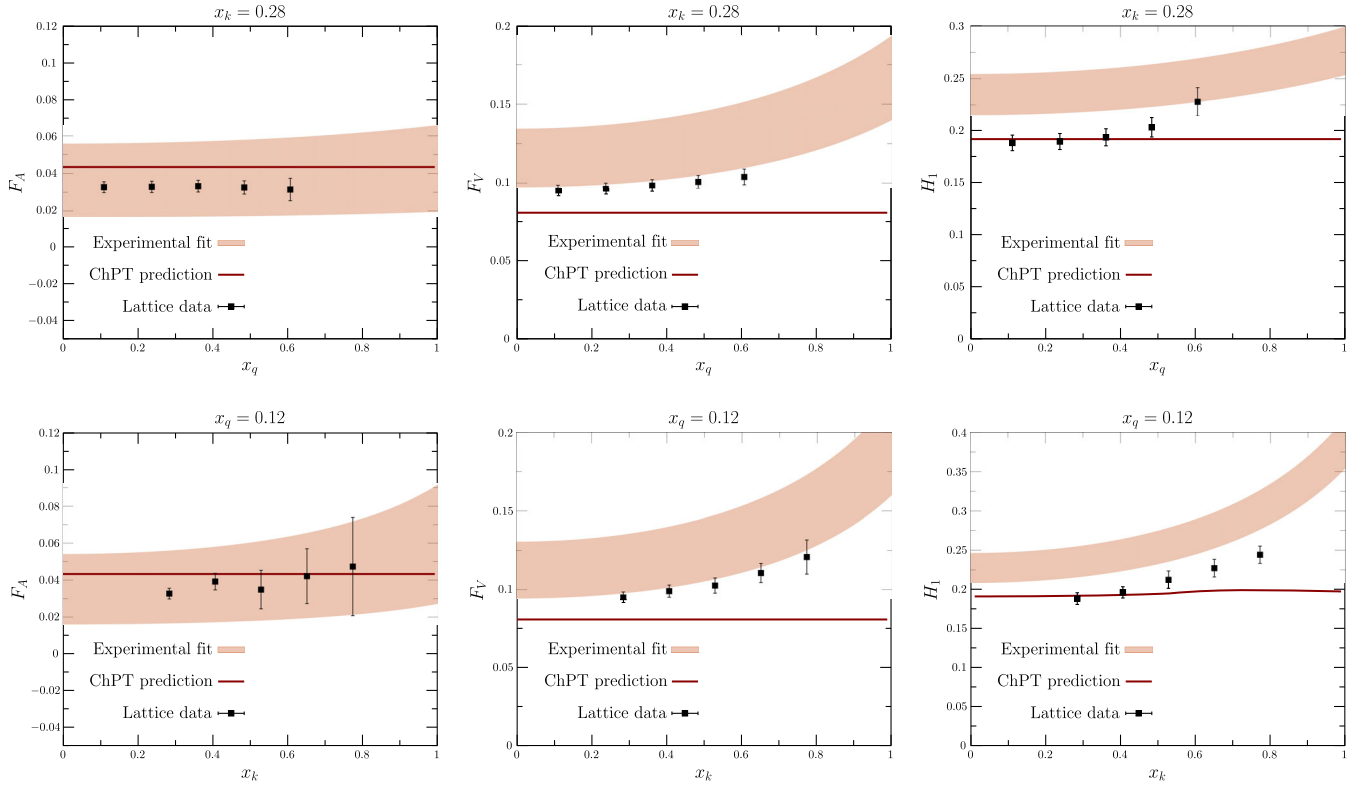

FIG. 10. The experimental VMD fits for the form factors H_1, F_A and F_V performed in Ref. [10] are plotted, together with our lattice data, as functions of x_q at a fixed value of $x_k = 0.28$ (top) and as functions of x_k at a fixed value of $x_q = 0.12$ (bottom). The red line corresponds to the one-loop ChPT prediction with $F = f_K/\sqrt{2}$.
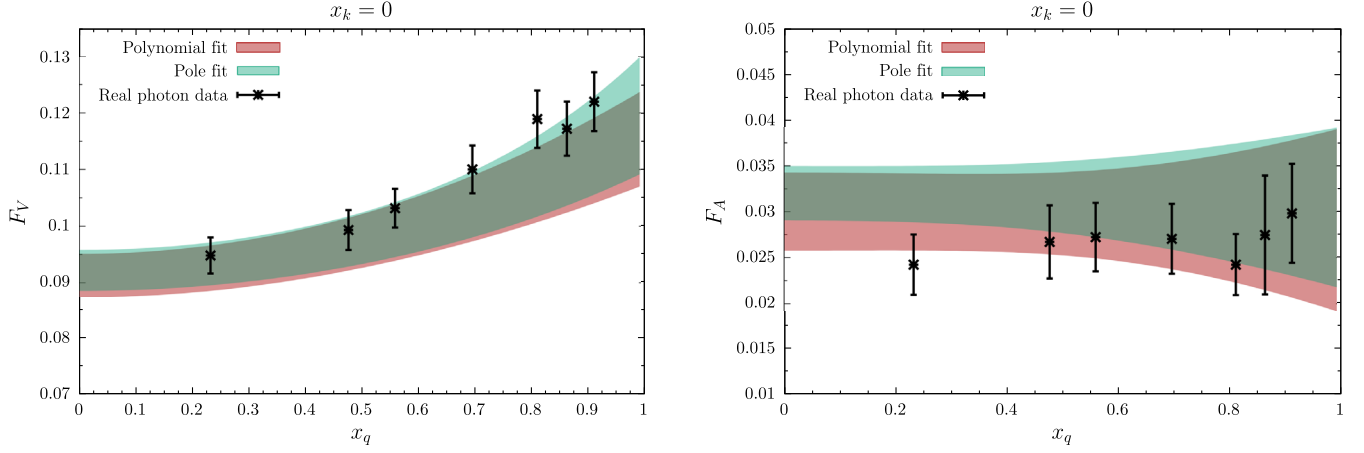
FIG. 11.   Extrapolation of our lattice results for F_V (left) and F_A (right) to $x_k = 0$ using the polynomial and pole fit *Ansätze* defined in Eqs. (46) and (47) (colored bands). The black points correspond to the lattice results for F_V and F_A obtained directly at $x_k = 0$ in our study of $K \to \ell \nu_\ell \gamma$ decays [7].

agreement with the prediction of Eq. (52).[6] Moreover, making use of Eq. (50) one has that the contribution from the intermediate kaon to H_2 at $x_k = 0$ is given by

$$H_{2;K^+}(x_k = 0) = f_K m_K \frac{\langle r_K^2 \rangle}{3}. \qquad (53)$$

Using the value from the PDG, $\langle r_K^2 \rangle = (0.560 \pm 0.031 \text{ fm})^2$ [9] and the physical values of the kaon mass and decay constant, one obtains $H_{2;K^+}(x_k = 0) = 0.206(23)$, which nicely agrees with the value we obtained for the parameter A in the pole-like fit of H_2 presented in Table II. Assuming the dominance of the rho-meson pole in the electromagnetic form factor F_V^K, one has that $H_2 \propto 1/(1 - R_k x_k^2)$ with $R_k = (m_K/m_\rho)^2 \simeq 0.4116$. In this case, our fitted value of R_k turns out to be larger than the value predicted by VMD.

We end this section by comparing the results for the form factors F_V and F_A obtained in this paper and extrapolated to $x_k = 0$ using Eqs. (46) and (47) with those reported on the same configurations in our earlier paper with a real photon in the final state, i.e., for the decays $K \to \ell \nu_\ell \gamma$.[7] The comparison is shown in Fig. 11 and shows good agreement, in spite of the fact that the *Ansätze* and parameters in Eqs. (46) and (47) were obtained from fits to data with $x_k \geq 0.28$.

---

[6]This depends on the choice we made in Eq. (5) for the kinematic prefactor in the definition of H_2 in the decomposition of the hadronic tensor in terms of form factors. If instead we had employed the same parametrization as in Ref. [17] or Ref. [19], we would have had a pole $1/(1 - x_q^2)$ in the expression in Eq. (52).

[7]The form factors H_1 and H_2 do not contribute to the amplitude for $K \to \ell \nu_\ell \gamma$ decays.

VI. $K^+ \to \ell^+ \nu_\ell \ell'^+ \ell'^-$ DECAY RATES

From the knowledge of the hadronic tensor $H^{\mu\nu}$, the $K^+ \to \ell^+ \nu_\ell \ell'^+ \ell'^-$ decay rate is obtained by integrating the square of the unpolarized amplitude, $\sum_{\text{spins}} |\mathcal{M}|^2$, over the phase space of the final-state charged leptons and neutrino. When the two positively charged leptons are different, i.e., when $\ell \neq \ell'$, the amplitude $\mathcal{M}$ is given by

$$\mathcal{M}(p_{\ell'+}, p_{\ell'-}, p_{\ell+}, p_{\nu_\ell})$$
$$= -\frac{G_F}{\sqrt{2}} V_{us}^* \frac{e^2}{k^2} \bar{u}(p_{\ell'-}) \gamma_\mu v(p_{\ell'+}) [f_K L^\mu(p_{\ell'+}, p_{\ell'-}, p_{\ell+}, p_{\nu_\ell})$$
$$- H_{\text{SD}}^{\mu\nu}(p,q) l_\nu(p_{\ell+}, p_{\nu_\ell})], \qquad (54)$$

where the leptonic vectors are given by

$$L^\mu(p_{\ell'+}, p_{\ell'-}, p_{\ell+}, p_{\nu_\ell})$$
$$= m_\ell \bar{u}(p_{\nu_\ell})(1 + \gamma_5) \left\{ \frac{2p^\mu - k^\mu}{2p \cdot k - k^2} - \frac{2p_{\ell+}^\mu + \slashed{k}\gamma^\mu}{2p_{\ell+} \cdot k + k^2} \right\} v(p_{\ell+}),$$
$$(55)$$

$$l^\mu(p_{\ell+}, p_{\nu_\ell}) = \bar{u}(p_{\nu_\ell}) \gamma^\mu (1 - \gamma_5) v(p_{\ell+}). \qquad (56)$$

In Eqs. (54)–(56), p is the four-momentum of the kaon, $k = p_{\ell'+} + p_{\ell'-}$, and $q = p_{\ell+} + p_{\nu_\ell}$. In Eq. (54), the first term in the square brackets gives the decay rate in the approximation in which the decaying kaon is treated as a point-like particle and includes the radiation from both the meson and charged lepton.[8] Except for the kaon decay constant f_K, the nonperturbative contribution to the rate is entirely contained in the second term of Eq. (54). The SD part of the hadronic tensor $H_{\text{SD}}^{\mu\nu}$ is defined in Eq. (5).

---

[8]This term is frequently referred to as the *inner-bremsstrahlung* contribution.

When $\ell = \ell'$, since the final-state positively charged leptons are indistinguishable, the exchange contribution, in which the momenta $p_{\ell'^+}$ and p_{ℓ^+} are interchanged, must be added to the amplitude $\mathcal{M}$ resulting in the replacement

$$\mathcal{M}(p_{\ell'^+}, p_{\ell'^-}, p_{\ell^+}, p_{\nu_\ell}) \rightarrow \mathcal{M}(p_{\ell'^+}, p_{\ell'^-}, p_{\ell^+}, p_{\nu_\ell}) - \mathcal{M}(p_{\ell^+}, p_{\ell'^-}, p_{\ell'^+}, p_{\nu_\ell}). \tag{57}$$

The branching ratio for $K^+ \rightarrow l^+\nu_l l'^+ l'^-$ decays is given by

$$\mathrm{BR}[K^+ \rightarrow l^+\nu_l l'^+ l'^-] = \frac{\mathcal{S}}{2m_K \Gamma_K (2\pi)^8} \int \sum_{\mathrm{spins}} |\mathcal{M}|^2 \delta(p - p_{l^+} - p_{\nu_l} - p_{l'^+} - p_{l'^-}) \frac{d^3 p_{l^+}}{2E_{l^+}} \frac{d^3 p_{\nu_l}}{2E_{\nu_l}} \frac{d^3 p_{l'^+}}{2E_{l'^+}} \frac{d^3 p_{l'^-}}{2E_{l'^-}}, \tag{58}$$

where $\Gamma_K = 5.3167(86) \times 10^{-17}$ GeV is the total decay rate of the K^+ meson [9] and $\mathcal{S}$ is a symmetry factor that takes the value $\mathcal{S} = 1$ for $\ell \neq \ell'$ and $\mathcal{S} = 1/2$ for $\ell = \ell'$. Since the phase-space integration is considerably easier for the case $\ell \neq \ell'$, in which a significant part of the integration can be performed analytically, we will discuss the two cases separately.

A. Decays with $\ell \neq \ell'$

When the final-state leptons have different flavors, the integral over the spatial momenta of the final-state particles can be partially performed analytically using invariance arguments and the fact that in $\sum_{\mathrm{spins}} |\mathcal{M}|^2$ the form factors only depend on $k^2 = (p_{\ell'^+} + p_{l'^-})^2$ and $q^2 = (p_{\ell^+} + p_{\nu_\ell})^2$ [30]. This leads to the following simplified expression for the differential decay rate [17]:

$$d\Gamma[K^+ \rightarrow \ell^+\nu_\ell \ell'^+ \ell'^-] = \alpha^2 G_F^2 |V_{us}|^2 m_K^5 2x_k x_q G(x_k, r_{\ell'}) \left\{ -\sum_{\mathrm{spins}} T_\mu^* T^\mu \right\} dx_k dx_q dy, \tag{59}$$

where

$$r_\ell = \frac{m_\ell^2}{m_K^2}, \qquad r_{\ell'} = \frac{m_{\ell'}^2}{m_K^2}, \qquad y = \frac{2p_\ell \cdot p}{m_K^2}, \qquad G(x_k, r_{\ell'}) = \frac{1}{192\pi^3 x_k^2} \left\{ 1 + \frac{2r_{\ell'}}{x_k^2} \right\} \sqrt{1 - \frac{4r_{\ell'}}{x_k^2}}, \qquad T^\mu = \frac{\sqrt{2}}{m_K^2} \{ f_K L^\mu - H_{\mathrm{SD}}^{\mu\nu} l_\nu \}. \tag{60}$$

The dimensionless integration variables x_k and x_q have been defined in Eq. (43). The integration domain is given by

$$A - B \leq y \leq A + B, \tag{61}$$

where

$$A = \frac{(2 - x_\gamma)(1 + x_k^2 + r_\ell - x_\gamma)}{2(1 + x_k^2 - x_\gamma)}, \qquad B = \frac{(1 + x_k^2 - x_\gamma - r_\ell)\sqrt{x_\gamma^2 - 4x_k^2}}{2(1 + x_k^2 - x_\gamma)}, \tag{62}$$

$$x_\gamma \equiv \frac{2p \cdot k}{m_K^2} = 1 + x_k^2 - x_q^2, \tag{63}$$

and the limits of integration for x_k and x_q are given in Eq. (45). Since the form factors only depend on the invariant mass of the lepton-antilepton pair ($x_k m_K$) and on the invariant mass of the lepton-neutrino pair ($x_q m_K$), the integral over the variable y can also be performed analytically, leaving the following expression for the double differential decay rate:

$$\frac{\partial^2}{\partial x_k \partial x_q} \Gamma[K^+ \rightarrow \ell^+\nu_\ell \ell'^+ \ell'^-] = \alpha^2 G_F^2 |V_{us}|^2 m_K^5 [\Gamma_{\mathrm{pt}}''(x_k, x_q) + \Gamma_{\mathrm{int}}''(x_k, x_q) + \Gamma_{\mathrm{SD}}''(x_k, x_q)]. \tag{64}$$
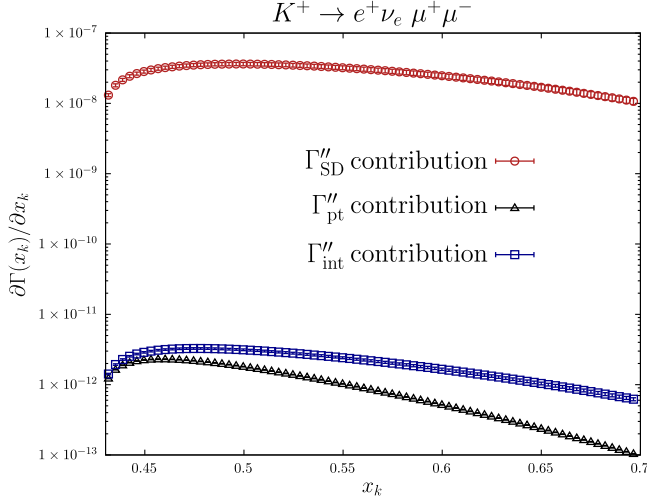
$$K^+ \to e^+ \nu_e \, \mu^+ \mu^-$$

FIG. 12. The contributions from Γ''_{pt}, Γ''_{int} and Γ''_{SD} to the differential rate $\partial\Gamma(x_k)/\partial x_k$, are shown for the decay channel $K^+ \to e^+\nu_e\mu^+\mu^-$. Although not shown in the figure, all contributions to $\partial\Gamma(x_k)/\partial x_k$ are zero at $x_k = 2\sqrt{r_\ell} \simeq 0.4280$ but grow rapidly as x_k is increased.

$$K^+ \to \mu^+ \nu_\mu \, e^+ e^-$$

FIG. 13. The contributions from Γ''_{pt}, Γ''_{int} and Γ''_{SD} to the differential rate $\partial\Gamma(x_k)/\partial x_k$, are shown for the decay channel $K^+ \to \mu^+\nu_\mu e^+e^-$. Even if not shown in the figure, all contributions to $\partial\Gamma(x_k)/\partial x_k$ are zero at $x_k = 2\sqrt{r_\ell} \simeq 0.00207$ but grow rapidly as x_k is increased.

The differential rate is written as a sum of three different contributions. The first term, $\Gamma''_{\mathrm{pt}}(x_k, x_q)$, is the point-like contribution proportional to f_K^2 and gives the total differential decay rate in the absence of any SD terms (i.e., if $H_{\mathrm{SD}}^{\mu\nu} = 0$). The third term, $\Gamma''_{\mathrm{SD}}(x_k, x_q)$, is the contribution to the decay rate coming entirely from $H_{\mathrm{SD}}^{\mu\nu}$, and corresponds to a quadratic expression of the form factors H_1, H_2, F_A, F_V. Finally, $\Gamma''_{\mathrm{int}}(x_k, x_q)$ is the interference term between the point-like and SD components of the amplitude. It arises from contributions of the form $H_{\mathrm{SD}}^{\mu\nu}L_\mu l_\nu$ in $T_\mu^* T^\mu$ and is proportional to f_K and depends linearly on the form factors. Clearly, all the information from the internal structure of the kaon (i.e., from $H_{\mathrm{SD}}^{\mu\nu}$) is contained in $\Gamma''_{\mathrm{int}}(x_k, x_q)$ and $\Gamma''_{\mathrm{SD}}(x_k, x_q)$. The Γ'' functions are all dimensionless quantities which can be evaluated directly from the knowledge of the form factors and of the dimensionless ratio f_K/m_K, for which we use our lattice value $f_K/m_K = 0.3057(11)$. Their explicit expressions in terms of H_1, H_2, F_A, F_V, and f_K/m_K are presented in
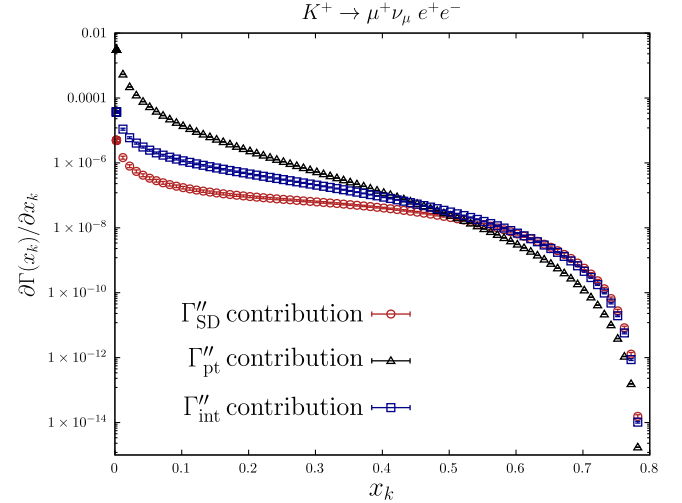
Appendix A. Using these formulas and the form factors obtained from the polynomial and pole-like fits described in the previous section, we are able to evaluate each of the terms on the right-hand side of Eq. (64). In order to obtain the total decay rates, we rely on numerical integration using Gaussian quadrature rules.

For the decay $K^+ \to e^+\nu_e\mu^+\mu^-$ the differential decay rate is completely dominated by the SD terms since the point-like contribution is helicity suppressed ($L_\mu \propto m_e$). This is shown in Fig. 12, where we plot, as functions of x_k, the contributions from Γ''_{pt}, Γ''_{int} and Γ''_{SD} to the partially integrated differential decay rate $\partial\Gamma(x_k)/\partial x_k = \int dx_q \partial^2\Gamma/\partial x_k \partial x_q$. Furthermore, we find that the dominant term in the integral of Γ''_{SD} is that proportional to H_1^2, while the contribution to the rate from the form factor H_2 turns out to be negligible. The remaining linear and quadratic terms in the form factors give subdominant contributions to the branching ratio of about 5% in total. Integrating the double differential decay rate of Eq. (64), we obtain the following value for the branching ratio:

TABLE IV. Comparison of our result for the branching ratio $\mathrm{BR}[K^+ \to e^+\nu_e\mu^+\mu^-]$ with the one coming from the point-like approximation, the result from Ref. [13] and the results for the branching ratio obtained using the NLO ChPT predictions for the SD form factors [Eq. (48)] setting either $F = f_\pi/\sqrt{2}$ or $F = f_K/\sqrt{2}$ [denoted by $\mathrm{ChPT}(f_\pi)$ and $\mathrm{ChPT}(f_K)$ respectively]. In the last column we show the experimental result from the E865 experiment [11]. We stress that both our lattice result and that from Ref. [13] are affected by systematic uncertainties due to the missing chiral, continuum and infinite-volume extrapolations.

$\mathrm{BR}[K^+ \to e^+\nu_e\mu^+\mu^-]$					
This work	Point-like approximation	Tuo *et al.* [13]	$\mathrm{ChPT}(f_\pi)$	$\mathrm{ChPT}(f_K)$	Experiment [11]
$0.762(49) \times 10^{-8}$	3.0×10^{-13}	$0.72(5) \times 10^{-8}$	1.19×10^{-8}	0.62×10^{-8}	$1.72(45) \times 10^{-8}$

TABLE V. Comparison of our result for the branching ratio BR[$K^+ \to \mu^+ \nu_\mu e^+ e^-$] with the one coming from the point-like approximation, the result from Ref. [13] and the results for the branching ratio obtained using the NLO ChPT predictions for the SD form factors [Eq. (48)] setting either $F = f_\pi/\sqrt{2}$ or $F = f_K/\sqrt{2}$ [denoted by ChPT(f_π) and ChPT(f_K) respectively]. In the last column we show the experimental result from the E865 experiment [10], which has been extrapolated from $x_k > 0.294$ to $x_k > 0.284$ using the formula presented in Ref. [10]. We stress that both our lattice result and that from Ref. [13] are affected by systematic uncertainties due to the missing chiral, continuum and infinite-volume extrapolations.

BR[$K^+ \to \mu^+ \nu_\mu e^+ e^-$] for $x_k > 0.284$					
This work	Point-like approximation	Tuo *et al.* [13]	ChPT(f_π)	ChPT(f_K)	Experiment [10]
$8.26(13) \times 10^{-8}$	4.8×10^{-8}	$10.59(33) \times 10^{-8}$	9.82×10^{-8}	8.25×10^{-8}	$7.93(33) \times 10^{-8}$

$$\mathrm{BR}[K^+ \to e^+ \nu_e \mu^+ \mu^-] = 0.762(49) \times 10^{-8}. \quad (65)$$

In Table IV we compare this result with the recent lattice value from Ref. [13], the predictions from ChPT and the measurement from the E865 experiment at the Brookhaven AGS [11]. As the table shows, our value of the branching ratio is in agreement with the updated determination of Ref. [13], while there is a tension with the experimental measurement at the level of about 2σ. However, it should be noted that both our computation and that of Ref. [13] are limited to a single value of the lattice spacing, a single volume and unphysically large light-quark masses. Given that the branching ratio is dominated by the quadratic term proportional to H_1^2 an increase of about 25% in the value of H_1, due to the missing continuum, chiral and infinite-volume extrapolations, would reduce the tension between our result and the experimental measurement to about 1σ. It will be very interesting in the future, once these extrapolations have been performed, to learn whether H_1 does indeed increase. We also note however, that there is a 1.6σ difference between the values of $H_1(0,0)$ obtained in Refs. [10,11]. The value of $H_1(0,0)$ deduced by the E865 Collaboration from the experimental study of the decay $K^+ \to e^+ \nu_e \mu^+ \mu^-$ is $H_1(0,0) = 0.303 \pm 0.043$ [11].[9] This value is somewhat higher than that also obtained, from studies of the decays $K^+ \to e^+ \nu_e e^+ e^-$ and $K^+ \to \mu^+ \nu_\mu e^+ e^-$ in the E865 experiment, $H_1(0,0) = 0.227 \pm 0.019$ [10], which is quoted in Table III.

For the decay channel $K^+ \to \mu^+ \nu_\mu e^+ e^-$, the point-like contribution is not helicity suppressed ($L_\mu \propto m_\mu$), and gives the dominant contribution to the differential decay rate at small values of the $e^+ e^-$ invariant mass. This is illustrated in Fig. 13, where we plot the contributions of $\Gamma''_{\rm pt}$, $\Gamma''_{\rm int}$ and $\Gamma''_{\rm SD}$ to the partially integrated differential decay rate $\partial\Gamma(x_k)/\partial x_k$. The contributions from $\Gamma''_{\rm pt}$ and $\Gamma''_{\rm int} + \Gamma''_{\rm SD}$ become of similar size at values of $x_k \simeq 0.3$–0.4, which corresponds approximately to the cut on the $e^+ e^-$ invariant mass $\sqrt{k^2} > 145, 150$ MeV ($x_k > 0.294, 0.304$) adopted in

the E865 experiment [10]. For such values of the cut on x_k, we find that the contribution to the decay rate from $\Gamma''_{\rm int}$ is greater than that of $\Gamma''_{\rm SD}$ and that the contribution from the form factor H_2 is again negligible. Imposing a cut on the $e^+ e^-$ invariant mass of $x_k > 0.284$, we obtain the following value for the branching ratio:

$$\mathrm{BR}[K^+ \to \mu^+ \nu_\mu e^+ e^-] = 8.26(13) \times 10^{-8}. \quad (66)$$

In Table V we compare our result for the branching ratio with the lattice determination of Ref. [13], the ChPT prediction and the experimental result of Ref. [10]. In this case we find a remarkable agreement with both the experimental result and the ChPT predictions, while the lattice result of Ref. [13] is a little larger than ours. In this case, since the inference term dominates over $\Gamma''_{\rm SD}$, systematic effects in our determination of the form factors, due to lattice artifacts and the unphysical quark masses, will only propagate linearly in the result for the branching ratio; for example an increase in H_1 of 20% would increase the branching ratio by about 7%.

B. Decays with $\ell = \ell'$

When the final-state leptons have the same flavor, the exchange contribution must be added as shown in Eq. (57). In this case $\sum_{\rm spins} |\mathcal{M}|^2$, depends on products of form factors evaluated at $k^2 = (p_{\ell'^+} + p_{\ell'^-})^2$ and $q^2 = (p_{\ell^+} + p_{\nu_\ell})^2$ as before, but also at the exchanged invariant masses $k'^2 = (p_{\ell^+} + p_{\ell'^-})^2$ and $q'^2 = (p_{\ell'^+} + p_{\nu_\ell})^2$. It is therefore not possible to analytically integrate as many variables as before. For the decay $K^+ \to \ell^+ \nu_\ell \ell'^+ \ell'^-$, the four-body phase space $d\Phi_4$ can be written in terms of five Lorentz-invariant quantities $x_k, x_q, y_{12}, y_{34}, \phi$ as [13]

$$d\Phi_4 = \frac{\mathcal{S}\lambda\omega m_K^4}{2^{14}\pi^6} dx_k dx_q dy_{12} dy_{34} d\phi, \quad (67)$$

where $\omega = 2x_k x_q$, the symmetry factor $\mathcal{S} = \frac{1}{2}$ for the case $\ell = \ell'$, $\lambda = \sqrt{(1 - x_k^2 - x_q^2)^2 - 4x_k^2 x_q^2}$ and the three additional integration variables y_{12}, y_{34} and ϕ, are defined as

---

[9]We have combined the different errors quoted in Eq. (7) of Ref. [11] in quadrature.

$$y_{12} \equiv \frac{2}{m_K^2 \lambda} (p_{\ell'-} - p_{\ell'+}) \cdot (p_{\ell+} + p_{\nu_\ell}),$$

$$y_{34} \equiv \frac{2}{m_K^2 \lambda} \left(\left(1 + \frac{r_\ell}{x_q^2}\right) p_{\nu_\ell} - \left(1 - \frac{r_\ell}{x_q^2}\right) p_{\ell+} \right) \cdot (p_{l'+} + p_{\ell'-}),$$

$$\sin\phi \equiv -\frac{16}{\lambda \omega m_K^4} \frac{1}{\sqrt{(\lambda_{12}^2 - y_{12}^2)(\lambda_{34}^2 - y_{34}^2)}} \epsilon_{\mu\nu\rho\sigma} p_{\ell'-}^\mu p_{\ell'+}^\nu p_{\nu_\ell}^\rho p_{\ell+}^\sigma$$

$$(68)$$

where

$$\lambda_{12} = \sqrt{1 - 4\frac{r'_\ell}{x_k^2}}, \qquad \lambda_{34} = 1 - \frac{r_\ell}{x_q^2}. \qquad (69)$$

The integration domain is given by

$$-\lambda_{12} \leq y_{12} \leq \lambda_{12}, \qquad -\lambda_{34} \leq y_{34} \leq \lambda_{34}, \qquad \phi \in [0, 2\pi], \qquad (70)$$

while for x_k and x_q the limits of integration are as defined in Eq. (45). In order to determine the decay rate, we have evaluated the square of the unpolarized amplitude, $\sum_{\text{spins}} |\mathcal{M}|^2$, in terms of the five integration variables using FeynCalc [31]. As for the case when $\ell \neq \ell'$, we decompose the differential rate as a sum of a point-like, an interference and a quadratic term (SD) in the form factors, i.e., as

$$\frac{\partial^5 \Gamma}{\partial x_k \partial x_q \partial y_{12} \partial y_{34} \partial \phi} = \alpha^2 G_F^2 |V_{us}|^2 m_K^5 [\Gamma_{\text{pt}}^{(5)}(x_k, x_q, y_{12}, y_{34}, \phi)$$
$$+ \Gamma_{\text{int}}^{(5)}(x_k, x_q, y_{12}, y_{34}, \phi)$$
$$+ \Gamma_{\text{SD}}^{(5)}(x_k, x_q, y_{12}, y_{34}, \phi)]. \qquad (71)$$

The explicit, very lengthy, expressions for the three contributions $\Gamma_{\text{pt}}^{(5)}$, $\Gamma_{\text{int}}^{(5)}$ and $\Gamma_{\text{SD}}^{(5)}$, written in terms of the five integration variables and the form factors, are not presented here but are available upon request from the authors. The total rate can be obtained through standard Monte Carlo integration of these expressions over the five-dimensional phase space. This has been done employing the GSL implementation of the VEGAS algorithm of Lepage [32].
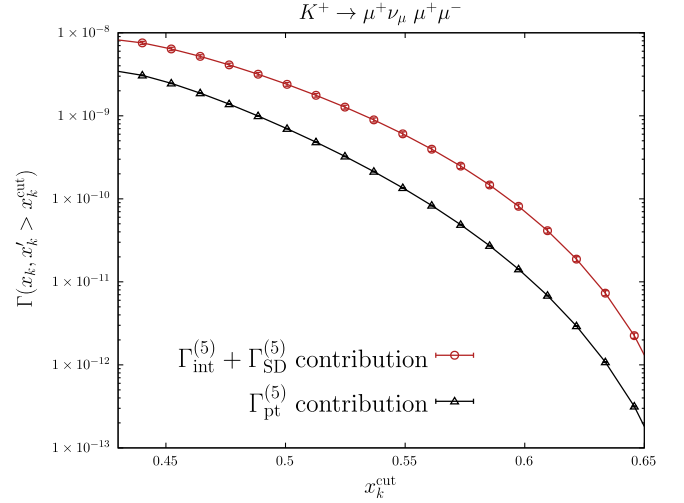

FIG. 14. The contributions from $\Gamma_{\text{pt}}^{(5)}$, and $\Gamma_{\text{int}}^{(5)} + \Gamma_{\text{SD}}^{(5)}$ to the integrated decay rate $\Gamma(x_k, x_{k'} > x_k^{\text{cut}})$ are shown for the decay channel $K^+ \to \mu^+ \nu_\mu \mu^+ \mu^-$, as functions of the common lower cut, x_k^{cut}, on the values of x_k and x_k'.

For the decay channel $K^+ \to \mu^+ \nu_\mu \mu^+ \mu^-$, we find that the point-like contribution corresponds to about 30% of the total rate. This is shown in Fig. 14, where we plot the contributions to the decay rate as a function of the lower cutoff on the invariant mass of the $\mu^+ \mu^-$ pair, from $\Gamma_{\text{pt}}^{(5)}$ alone and from $\Gamma_{\text{int}}^{(5)} + \Gamma_{\text{SD}}^{(5)}$. For decays into identical leptons, the same cuts are always applied to both invariant masses

$$\sqrt{k^2} = m_K x_k = \sqrt{(p_{\ell'+} + p_{\ell'-})^2},$$
$$\sqrt{k'^2} \equiv m_K x_k' = \sqrt{(p_{\ell+} + p_{\ell-})^2}. \qquad (72)$$

We find that the contribution from the form factor H_2 is again negligible and that the contribution from the vector form factor F_V is also very small. For the total branching ratio, we obtain the value

$$\text{BR}[K^+ \to \mu^+ \nu_\mu \mu^+ \mu^-] = 1.178(35) \times 10^{-8}. \qquad (73)$$

Since for this decay channel there is no experimental measurement available, our result can only be compared

TABLE VI. Comparison of our result for the branching ratio $\text{BR}[K^+ \to \mu^+ \nu_\mu \mu^+ \mu^-]$ with the one coming from the point-like approximation, the result from Ref. [13] and the results for the branching ratio obtained using the NLO ChPT predictions for the SD form factors [Eq. (48)] setting either $F = f_\pi/\sqrt{2}$ or $F = f_K/\sqrt{2}$ [denoted by ChPT(f_π) and ChPT(f_K) respectively]. We stress that both our lattice result and that from Ref. [13] are affected by systematic uncertainties due to the missing chiral, continuum and infinite-volume extrapolations.

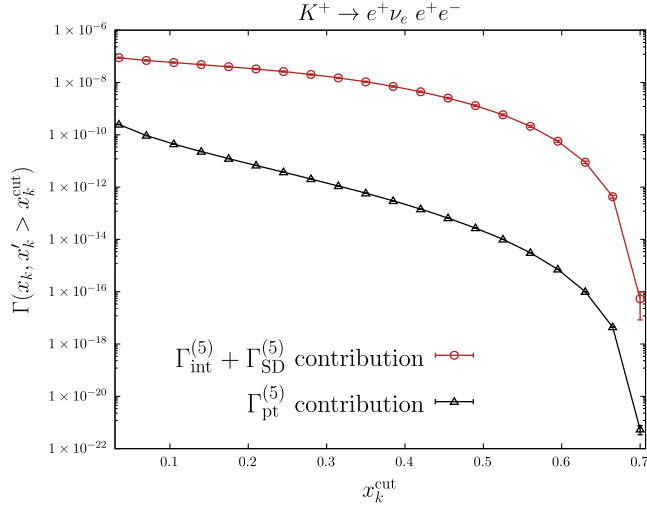| $\text{BR}[K^+ \to \mu^+ \nu_\mu \mu^+ \mu^-]$					
This work	Point-like approximation	Tuo *et al.* [13]	ChPT(f_π)	ChPT(f_K)	Experiment
$1.178(35) \times 10^{-8}$	3.7×10^{-9}	$1.45(6) \times 10^{-8}$	1.51×10^{-8}	1.10×10^{-8}	$\cdots$

FIG. 15.   The contributions from $\Gamma_{\rm pt}^{(5)}$, and $\Gamma_{\rm int}^{(5)} + \Gamma_{\rm SD}^{(5)}$ to the integrated decay rate $\Gamma(x_k, x_{k'} > x_k^{\rm cut})$ are shown for the decay channel $K^+ \to e^+ \nu_e e^+ e^-$, as functions of the common lower cut $x_k^{\rm cut}$ on the values of x_k and x_k'.

with the lattice determination of Ref. [13] and with the ChPT prediction (Table VI). As the table shows, our result is in reasonably good agreement with the value predicted by ChPT, while at this stage the observed discrepancy with the result obtained by Tuo *et al.* [13], which is of $\mathcal{O}(25\%)$ may perhaps be attributed to the unknown systematics associated with the missing chiral, continuum and infinite-volume extrapolations.

Finally, for the decay channel $K^+ \to e^+ \nu_e e^+ e^-$, we find again that the point-like contribution is much suppressed compared to that from the SD terms. This is shown in Fig. 15, where we plot, as in the previous case, the contribution from $\Gamma_{\rm pt}^{(5)}$ and $\Gamma_{\rm int}^{(5)} + \Gamma_{\rm SD}^{(5)}$ to the total decay rate, as a function of the lower cutoff on the $e^+ e^-$ invariant masses. Similarly to the case of the decay $K^+ \to \mu^+ \nu_\mu e^+ e^-$, we find that the dominant contribution to the rate is given by the term proportional to H_1^2, while the contributions from the form factors H_2 and F_V are very small. Employing the cutoffs $x_k, x_k' > 0.284$, we obtain the following value for the branching ratio:

$$\mathrm{BR}[K^+ \to e^+ \nu_e e^+ e^-] = 1.95(11) \times 10^{-8}. \qquad (74)$$

In Table VII we compare our determination with the experimental measurement of Ref. [10], the lattice result of Ref. [13], and the ChPT prediction. Our result appears to be significantly smaller than the experimental measurement, as in the case of the $K^+ \to \mu^+ \nu_\mu e^+ e^-$ decay, while being consistent with the updated determination of Ref. [13]. Since the term proportional to H_1^2 is also the dominant one in this case, this finding is consistent with possible systematic effects of about 20% on our lattice value.

VII. CONCLUSIONS

In this paper we have presented a strategy to compute, using lattice QCD, the amplitudes and branching ratios for the decays $P \to \ell \nu_\ell \ell'^+ \ell'^-$, where P is a pseudoscalar meson and ℓ and ℓ' are charged leptons. In particular, we explained how the four structure-dependent form factors can be determined and separated from the point-like ("inner-bremsstrahlung") contribution. Apart from a factor of the leptonic decay constant f_P, the point-like contribution to the amplitude can be calculated in perturbation theory, whereas the SD form factors are nonperturbative and describe the interaction of a generic off-shell photon with the internal hadronic structure of the meson. The present work, studying decays with the emission of a virtual photon, is a natural extension to our recent study of radiative decays $P \to \ell \nu_\ell \gamma$, with a real photon in the final state [7] and the subsequent detailed comparison to experimental results [8].

We applied the formalism developed in Secs. II–IV to the four channels of $K \to \ell \nu_\ell \ell'^+ \ell'^-$ decays, where ℓ and $\ell' = \mu$ or e, in an exploratory lattice QCD computation at a single lattice spacing and at unphysical light-quark masses. We demonstrated that all four SD form factors, F_V, F_A, H_1 and H_2 can be determined with good precision and used to calculate the corresponding branching ratios. In spite of the unphysical quark masses used in this simulation (our pion and kaon masses are about 320 and 530 MeV respectively), it has been interesting and instructive to compare our results with those from experiment (where available) and NLO ChPT. Perhaps surprisingly, as can be

TABLE VII.   Comparison of our result for the branching ratio $\mathrm{BR}[K^+ \to e^+ \nu_e e^+ e^-]$ with the one coming from the point-like approximation, the result from Ref. [13] and the results for the branching ratio obtained using the NLO ChPT predictions for the SD form factors [Eq. (48)] setting either $F = f_\pi/\sqrt{2}$ or $F = f_K/\sqrt{2}$ [denoted by ChPT(f_π) and ChPT(f_K) respectively]. In the last column we show the experimental result from the E865 experiment [10], which has been extrapolated from $x_k > 0.304$ to $x_k > 0.284$ using the formula presented in Ref. [10]. We stress that both our lattice result and that from Ref. [13] are affected by systematic uncertainties due to the missing chiral, continuum and infinite-volume extrapolations.

$\mathrm{BR}[K^+ \to e^+ \nu_e e^+ e^-]$ for $x_k > 0.284$					
This work	Point-like approximation	Tuo *et al.* [13]	ChPT(f_π)	ChPT(f_K)	Experiment [10]
$1.95(11) \times 10^{-8}$	2.0×10^{-12}	$1.77(16) \times 10^{-8}$	3.34×10^{-8}	1.75×10^{-8}	$2.91(23) \times 10^{-8}$

seen from Tables IV–VII, the results are generally in reasonable semiquantitative agreement.

The comparison of our results with those from experimental measurements results in an interesting observation to be investigated further in the future. For the decays $K^+ \to e^+ \nu_e \mu^+ \mu^-$ and $K^+ \to e^+ \nu_e e^+ e^-$ the point-like contribution is negligible as a result of the chiral suppression due to the small electron mass, and the decay rate is dominated by the form factor H_1. In both cases our results are somewhat below the experimental measurement (see Tables IV and VII) and it would require an increase of order 20% in the value of H_1 to recover consistency.[10] It will be interesting to see whether such an increase will result after the continuum, chiral and infinite-volume extrapolations have been performed in the future.

A complementary exploratory lattice computation of the branching ratios has been performed by Tuo *et al.* [13] on a $24^3 \times 48$ lattice, with lattice spacing $a = 0.093$ fm and with quark masses similar to ours ($m_\pi = 352$ MeV and $m_K = 506$ MeV). The action with Wilson-clover twisted-mass fermions is different than the one we used which does not include the clover term. The methodology in Ref. [13] is also different than ours in that the individual form factors are not extracted and the point-like contribution is not separated from structure-dependent terms. The aim of our paper on the other hand, has been to explicitly determine the (nonperturbative) structure-dependent contributions to the decay rate. In Tables IV–VII we also compared our results with those of Ref. [13], but given the different systematics, and in particular the finite-volume effects, we did not speculate on the origin of any differences.

Having demonstrated the feasibility of the method, our future work will focus on controlling and reducing the systematic uncertainties and in particular those resulting from the current absence of continuum, chiral and infinite-volume extrapolations. We will also work to extend the method to heavier pseudoscalar mesons, for which the analytic continuation to Euclidean space gives rise to

enhanced finite-volume effects due to the presence of internal lighter states. Given the recent results suggesting the violation of lepton-flavor universality and potential new interactions involving leptons (see e.g., Ref. [2] for a brief introduction), we believe that reliable nonperturbative, model-independent theoretical predictions of decays such as those studied here will be very useful in unraveling the underlying theory beyond the Standard Model. In particular, experimental measurements of ratios of decay rates of heavy mesons into different final-state leptons, together with the corresponding lattice calculations, would be a significant contribution to the general investigation of lepton-flavor universality.

APPENDIX A: FORMULAS FOR THE DECAY RATES WHEN $\ell \neq \ell'$

In this appendix, we present the functions which multiply the form factors in the differential decay rates we computed in Sec. VI A, with different charged leptons in the final state, i.e., for $\ell \neq \ell'$.

We start by defining the following quantity:

$$\Delta_{\log}(x_k, x_q)$$
$$= \log\left(1 + 2\frac{x_q^2\sqrt{x_k^4 - 2x_k^2(x_q^2+1) + (x_q^2-1)^2} - r_\ell\sqrt{-2(x_k^2+1)x_q^2 + (x_k^2-1)^2 + x_q^4}}{-x_q^2\sqrt{x_k^4 - 2x_k^2(x_q^2+1) + (x_q^2-1)^2} + r_\ell\sqrt{-2(x_k^2+1)x_q^2 + (x_k^2-1)^2 + x_q^4} + r_\ell(x_k^2-1) + x_q^2(-x_k^2+x_q^2+r_\ell-1)}\right),$$
$$\tag{A1}$$

where x_k and x_q are defined in Eq. (43) and r_ℓ is defined in Eq. (60).

---

[10]Note also the discrepancy in the values of $H_1(0,0)$ in Refs. [10,11] obtained in the E865 experiment. This is discussed in Sec. VI A.

The point-like contribution to the decay rate is given by

$$\Gamma_{\text{pt}}''(x_k, x_q) = \frac{f_K^2 r_\ell x_q}{24\pi^3 m_K^3 x_k}\sqrt{1 - \frac{4r_{\ell'}}{x_k^2}}\left(\frac{2r_{\ell'}}{x_k^2} + 1\right)\left(\frac{2}{x_q^2 - 1}(-x_k^2 x_q^2 + x_k^2 + x_q^4 - 2x_q^2 r_\ell - 2(r_\ell - 1)r_\ell + 1)\Delta_{\log}(x_k, x_q)\right.$$

$$\left.+ \sqrt{(x_k^2 - x_q^2 + 1)^2 - 4x_k^2}(x_q^2 - r_\ell)\left(\frac{x_k^2 x_q^2 - x_k^2 r_\ell - 2x_q^4 + 4x_q^2 r_\ell - 2}{(x_q^2 - 1)^2 x_q^2} + \frac{2(r_\ell - 1)(x_k^2 + 2r_\ell)}{(x_q^2 - 1)^2 r_\ell - x_k^2(r_\ell - 1)(x_q^2 - r_\ell)}\right)\right),$$

(A2)

where $r_{\ell'}$ is also defined in Eq. (60).

The interference contribution to the decay rate can be expressed in the form

$$\Gamma_{\text{int}}''(x_k, x_q) = [g_V(x_k, x_q)F_V(x_k, x_q) + g_A(x_k, x_q)F_A(x_k, x_q) + g_1(x_k, x_q)H_1(x_k, x_q) + g_2(x_k, x_q)H_2(x_k, x_q)], \quad \text{(A3)}$$

where the interference kernels are

$$g_V(x_k, x_q) = \frac{f_K r_\ell x_q}{12\pi^3 m_K x_k}\sqrt{1 - \frac{4r_{\ell'}}{x_k^2}}\left(\frac{2r_{\ell'}}{x_k^2} + 1\right)\left\{(x_k^2(x_q^2 - 2r_\ell + 1) - (x_q^2 - 1)^2)\Delta_{\log}(x_k, x_q)\right.$$

$$\left.+ \frac{(x_k^2 + x_q^2 - 1)(x_q^2 - r_\ell)\sqrt{(x_k^2 - x_q^2 + 1)^2 - 4x_k^2}}{x_q^2}\right\},$$

$$g_A(x_k, x_q) = \frac{f_K r_\ell x_q}{12\pi^3 m_K x_k(x_q^2 - 1)}\sqrt{1 - \frac{4r_{\ell'}}{x_k^2}}\left(\frac{2r_{\ell'}}{x_k^2} + 1\right)\left\{(x_q^2 - 1)^2(-x_k^2 - x_q^2 - 2r_\ell + 1)\Delta_{\log}(x_k, x_q)\right.$$

$$\left.+ \frac{(x_q^2 - 1)(x_q^2 - r_\ell)(x_k^2 + 2x_q^2 + r_\ell - 1)\sqrt{-2(x_k^2 + 1)x_q^2 + (x_k^2 - 1)^2 + x_q^4}}{x_q^2}\right\},$$

$$g_1(x_k, x_q) = \frac{f_K r_\ell x_k x_q}{24\pi^3 m_K}\sqrt{1 - \frac{4r_{\ell'}}{x_k^2}}\left(\frac{2r_{\ell'}}{x_k^2} + 1\right)\left\{4(x_q^2 + r_\ell - 2)\Delta_{\log}(x_k, x_q)\right.$$

$$\left.- \frac{(x_q^2 - r_\ell)(r_\ell(-x_k^2 + 3x_q^2 + 1) + x_q^2(x_k^2 + 5x_q^2 - 9))\sqrt{-2(x_k^2 + 1)x_q^2 + (x_k^2 - 1)^2 + x_q^4}}{(x_q^2 - 1)x_q^4}\right\},$$

$$g_2(x_k, x_q) = \frac{f_K r_\ell x_k x_q}{24\pi^3 m_K(x_q^2 - 1)^2}\sqrt{1 - \frac{4r_{\ell'}}{x_k^2}}\left(\frac{2r_{\ell'}}{x_k^2} + 1\right)\left\{2(x_q^2 - 1)(x_q^2 - r_\ell^2)\Delta_{\log}(x_k, x_q)\right.$$

$$\left.- \frac{(x_q^2 - r_\ell)(r_\ell(x_k^2 - 3x_q^2 - 1) + x_q^2(-x_k^2 + x_q^2 + 3))\sqrt{(x_k^2 - x_q^2 + 1)^2 - 4x_k^2}}{x_q^2}\right\}.$$

(A4)

The SD contribution to the decay rate can be expressed in the form

$$\Gamma_{\text{SD}}''(x_k, x_q) = g_{VV}(x_k, x_q)F_V^2(x_k, x_q) + g_{AA}(x_k, x_q)F_A^2(x_k, x_q) + g_{11}(x_k, x_q)H_1^2(x_k, x_q) + g_{22}(x_k, x_q)H_2^2(x_k, x_q)$$

$$+ g_{A1}(x_k, x_q)F_A(x_k, x_q)H_1(x_k, x_q) + g_{12}(x_k, x_q)H_1(x_k, x_q)H_2(x_k, x_q), \quad \text{(A5)}$$

where the SD kernels are

$$g_{VV}(x_k, x_q) = \frac{1}{24\pi^3 x_k x_q} \sqrt{1 - \frac{4r_{\ell'}}{x_k^2}} \left(\frac{2r_{\ell'}}{x_k^2} + 1\right) ((x_k^2 - x_q^2 + 1)^2 - 4x_k^2)^{3/2} (x_q^2 - r_\ell)^2,$$

$$g_{AA}(x_k, x_q) = \frac{1}{144\pi^3 x_k x_q^3} \sqrt{1 - \frac{4r_{\ell'}}{x_k^2}} \left(\frac{2r_{\ell'}}{x_k^2} + 1\right) (x_k^4 + x_k^2(4x_q^2 - 2) + (x_q^2 - 1)^2)(x_q^2 - r_\ell)^2 (2x_q^2 + r_\ell)$$
$$\times \sqrt{(x_k^2 - x_q^2 + 1)^2 - 4x_k^2},$$

$$g_{11}(x_k, x_q) = \frac{x_k}{144\pi^3 x_q^5} \sqrt{1 - \frac{4r_{\ell'}}{x_k^2}} \left(\frac{2r_{\ell'}}{x_k^2} + 1\right) (x_q^2 - r_\ell)^2 \sqrt{(x_k^2 - x_q^2 + 1)^2 - 4x_k^2}$$
$$\times (2x_q^4(5x_k^2 + r_\ell - 1) + x_q^2(2(x_k^2 - 2)r_\ell + (x_k^2 - 1)^2) + 2(x_k^2 - 1)^2 r_\ell + x_q^6),$$

$$g_{22}(x_k, x_q) = \frac{r_\ell x_k}{96\pi^3 (x_q^2 - 1)^2 x_q} \sqrt{1 - \frac{4r_{\ell'}}{x_k^2}} \left(\frac{2r_{\ell'}}{x_k^2} + 1\right) ((x_k^2 - x_q^2 + 1)^2 - 4x_k^2)^{3/2} (x_q^2 - r_\ell)^2,$$

$$g_{A1}(x_k, x_q) = -\frac{x_k}{24\pi^3 x_q^3} \sqrt{1 - \frac{4r_{\ell'}}{x_k^2}} \left(\frac{2r_{\ell'}}{x_k^2} + 1\right) (x_k^2 + x_q^2 - 1)(x_q^2 - r_\ell)^2 (2x_q^2 + r_\ell) \sqrt{(x_k^2 - x_q^2 + 1)^2 - 4x_k^2},$$

$$g_{12}(x_k, x_q) = -\frac{r_\ell x_k}{48\pi^3 (x_q^2 - 1)x_q^3} \sqrt{1 - \frac{4r_{\ell'}}{x_k^2}} \left(\frac{2r_{\ell'}}{x_k^2} + 1\right) ((x_k^2 - x_q^2 + 1)^2 - 4x_k^2)^{3/2} (x_q^2 - r_\ell)^2. \tag{A6}$$

APPENDIX B: THREE-POINT CORRELATION FUNCTION IN THE INFRARED LIMIT $k \to 0$

In this appendix, we study the behavior of the lattice Euclidean correlation function $C^{\mu\nu}(t, E_\gamma, \boldsymbol{k}, \boldsymbol{p})$ in the limit $k \to 0$ which, as we will see below, is nontrivial. From spectral decomposition one obtains

$$C^{\mu\nu}(t, E_\gamma, \boldsymbol{k}, \boldsymbol{p}) = c_1^{\mu\nu} e^{-tE_P(\boldsymbol{p})} + c_2^{\mu\nu} e^{-t\{E_P(\boldsymbol{p}-\boldsymbol{k})+E_\gamma\}} + \cdots, \tag{B1}$$

where the dots represent exponentially suppressed contributions with an energy gap which, in the soft-photon limit, is or order $2m_\pi$. The first exponential corresponds to the on-shell external meson $P(\boldsymbol{p})$ with spatial momentum $\boldsymbol{p}$, and gives the contribution we aim to isolate, while the second exponential corresponds to the $P(\boldsymbol{p}-\boldsymbol{k}) + \gamma$ state, composed of an on-shell meson $P(\boldsymbol{p}-\boldsymbol{k})$ with spatial

momentum $\boldsymbol{p} - \boldsymbol{k}$, and a virtual photon with spatial momentum $\boldsymbol{k}$ and off-shell energy E_γ. When either $\boldsymbol{k}$ or E_γ are nonzero, it is possible to isolate the matrix element corresponding to the ground state $P(\boldsymbol{p})$, since the second exponential in Eq. (B1) is subleading at large time separations t. However, in the exact limit $k \to 0$, the energy-gap between the two states vanishes, and the lattice Euclidean correlator $C^{\mu\nu}(t, 0, \boldsymbol{0}, \boldsymbol{p})$ has a nontrivial behavior which we now discuss, paying special attention to the leading cutoff effects. This was already done for $P \to \ell\nu_\ell\gamma$ decays, with the emission of a real photon, in Appendix C of Ref. [7], focusing on the spatial components of $C^{\mu\nu}$, which are the only ones relevant in that case. In this appendix we generalize the analysis of Ref. [7] to the components $C^{0\nu}$ and $C^{\mu 0}$, with $\mu, \nu = 0, 1, 2, 3$.

The starting point is the electromagnetic Ward identity which, for Wilson-like fermions adopted in this study, reads [7]

$$\sum_{\mu=0}^{3} \frac{2}{a} \sin(ak_\mu/2) C_A^{\mu\nu}(t, k, \boldsymbol{p}) = C_A^\nu(t, \boldsymbol{p}) - C_A^\nu(t, E_\gamma, \boldsymbol{p} - \boldsymbol{k}), \tag{B2}$$

where we have defined

$$C_A^{\mu\nu}(t, k, \boldsymbol{p}) = -i \int d^4y \, d^3x \, e^{-ik\cdot(y+\hat{\mu}/2)-i\boldsymbol{p}\cdot\boldsymbol{x}} \langle 0|T[J_A^\nu(0)J_{\text{em}}^\mu(y)P(-t, -\boldsymbol{x})]|0\rangle, \tag{B3}$$

$$C_A^\nu(t, \boldsymbol{p}) = \int d^3x \, e^{-i\boldsymbol{p}\cdot\boldsymbol{x}} \langle 0|T[J_A^\nu(0)P(-t,-\boldsymbol{x})]|0\rangle = p^\nu \frac{\hat{f}_P(\boldsymbol{p})\hat{G}_P(\boldsymbol{p})}{2\hat{E}_P(\boldsymbol{p})} e^{-t\hat{E}_P(\boldsymbol{p})} + \cdots,$$

(B4)

$$C_A^\nu(t, \hat{E}_\gamma, \boldsymbol{p} - \boldsymbol{k}) = e^{-\hat{E}_\gamma t} \int d^3x \, e^{-i(\boldsymbol{p}-\boldsymbol{k})\cdot\boldsymbol{x}} \langle 0|T[J_A^\nu(0)P(-t,-\boldsymbol{x})]|0\rangle$$

$$= u^\nu \frac{\hat{f}_P(\boldsymbol{p}-\boldsymbol{k})\hat{G}_P(\boldsymbol{p}-\boldsymbol{k})}{2\hat{E}_P(\boldsymbol{p}-\boldsymbol{k})} e^{-t\hat{E}_P(\boldsymbol{p}-\boldsymbol{k})-t\hat{E}_\gamma} + \cdots,$$

(B5)

and where the ellipsis represents subleading exponentials with an energy gap that, in the infrared limit, starts at order $2m_\pi$.[11] In Eqs. (B3)–(B5) the integrals are to be read as lattice sums, $k = (i\hat{E}_\gamma, \boldsymbol{k})$ is the Euclidean four-momentum of the photon, the photon's four-momentum, while the on-shell (Euclidean) four-momenta of the mesons $P(\boldsymbol{p})$ and $P(\boldsymbol{p} - \boldsymbol{k})$ are given respectively by

$$p = (i\hat{E}_P(\boldsymbol{p}), \boldsymbol{p}), \qquad u = (i\hat{E}_P(\boldsymbol{p} - \boldsymbol{k}), \boldsymbol{p} - \boldsymbol{k}).$$

(B6)

In the previous expressions, the hat symbol denotes lattice quantities, which are related to their continuum counterparts by[12]

$$\hat{f}_P(\boldsymbol{p}) = f_P + O(a^2), \qquad \hat{G}_P(\boldsymbol{p}) = G_P + O(a^2), \qquad \hat{E}_P(\boldsymbol{p}) = E_P + O(a^2), \qquad \hat{E}_\gamma = E_\gamma + O(a^2),$$

(B7)

where $f_P, G_P, E_P(\boldsymbol{p})$ and E_γ are respectively the continuum decay constant, the continuum matrix element of the pseudoscalar density used as the interpolating operator ($G_P = \langle 0|P|P(\boldsymbol{p})\rangle$), and the continuum energy of the meson and of the virtual photon.

We now differentiate Eq. (B2) with respect to k^μ and then set $k = 0$. Since we are considering a generic off-shell photon, the temporal and spatial components of the photon momentum k^μ are treated as independent quantities. When the indices μ and ν are spatial, one obtains the result quoted in Eq. (C17) of Ref. [7],

$$C_A^{ij}(t, 0, \boldsymbol{p}) = \frac{\hat{f}_P(\boldsymbol{p})\hat{G}_P(\boldsymbol{p})}{2\hat{E}_P(\boldsymbol{p})} e^{-t\hat{E}_P(\boldsymbol{p})} \left\{ \delta^{ij} + p^j \left[\frac{1}{\hat{f}_P(\boldsymbol{p})} \frac{\partial \hat{f}_P(\boldsymbol{p})}{\partial p^i} + \frac{1}{\hat{G}_P(\boldsymbol{p})} \frac{\partial \hat{G}_P(\boldsymbol{p})}{\partial p^i} - \left(t + \frac{1}{\hat{E}_P(\boldsymbol{p})} \right) \frac{\partial \hat{E}_P(\boldsymbol{p})}{\partial p^i} \right] \right\} + \cdots$$

(B8)

Moreover the $H(3)$ symmetry of the lattice implies

$$\frac{\partial \hat{f}_P(\boldsymbol{p})}{\partial p^i} = p^i \times O(a^2), \qquad \frac{\partial \hat{G}_P(\boldsymbol{p})}{\partial p^i} = p^i \times O(a^2), \qquad \frac{\partial \hat{E}_P(\boldsymbol{p})}{\partial p^i} = \frac{p^i}{E_P(\boldsymbol{p})} \times (1 + O(a^2))$$

(B9)

so that

$$C_A^{ij}(t, 0, \boldsymbol{p}) = \frac{\hat{f}_P(\boldsymbol{p})\hat{G}_P(\boldsymbol{p})}{2\hat{E}_P(\boldsymbol{p})} e^{-t\hat{E}_P(\boldsymbol{p})} \left\{ \delta^{ij} - \frac{p^i p^j}{\hat{E}_P^2(\boldsymbol{p})} (1 + t\hat{E}_P(\boldsymbol{p}) + O(a^2)) \right\} + \cdots$$

(B10)

In the rest frame of the meson, $\boldsymbol{p} = 0$, which we use in our study, we therefore obtain for the spatial components of the correlation function

$$C_A^{ij}(t, 0, \boldsymbol{0}) = \delta^{ij} \frac{\hat{f}_P(\boldsymbol{0})\hat{G}_P(\boldsymbol{0})}{2\hat{E}_P(\boldsymbol{0})} e^{-t\hat{E}_P(\boldsymbol{0})} + \cdots$$

(B11)

For the component C_A^{00} the same procedure gives

$$C_A^{00}(t, 0, \boldsymbol{p}) = -t\hat{E}_P(\boldsymbol{p}) \frac{\hat{f}_P(\boldsymbol{p})\hat{G}_P(\boldsymbol{p})}{2\hat{E}_P(\boldsymbol{p})} e^{-t\hat{E}_P(\boldsymbol{p})} + \cdots$$

(B12)

---

[11]We take this opportunity to correct a typographical mistake in Eq. (C6) of Ref. [7]. In that equation, the factor $e^{E_\gamma t}$ should be replaced by $e^{-E_\gamma t}$. This is the corresponding factor to $e^{-\hat{E}_\gamma t}$ in the first line of Eq. (B5) above.
[12]In our twisted-mass formulation, cutoff effects on parity-even observables start at order $\mathcal{O}(a^2)$.

For the components C_A^{i0}, for the correlation function with J_A^0 and J_{em}^i, we obtain

$$C_A^{i0}(t,0,\boldsymbol{p})$$

$$=\frac{\hat{f}_P(\boldsymbol{p})\hat{G}_P(\boldsymbol{p})}{2\hat{E}_P(\boldsymbol{p})}e^{-t\hat{E}_P(\boldsymbol{p})}$$

$$\times\hat{E}_P(\boldsymbol{p})\left[\frac{1}{\hat{f}_P(\boldsymbol{p})}\frac{\partial\hat{f}_P(\boldsymbol{p})}{\partial p^i}+\frac{1}{\hat{G}_P(\boldsymbol{p})}\frac{\partial\hat{G}_P(\boldsymbol{p})}{\partial p^i}-t\frac{\partial\hat{E}_P(\boldsymbol{p})}{\partial p^i}\right]+\cdots$$

$$=-\frac{\hat{f}_P(\boldsymbol{p})\hat{G}_P(\boldsymbol{p})}{2\hat{E}_P(\boldsymbol{p})}e^{-t\hat{E}_P(\boldsymbol{p})}\times\hat{E}_P(\boldsymbol{p})p^i(t+O(a^2))+\cdots,$$

$$(B13)$$

which in our reference frame becomes

$$C_A^{i0}(t,0,\boldsymbol{0})=0+\cdots \qquad (B14)$$

Similarly, for the components C_A^{0i}, differentiating equation Eq. (B2) results in

$$C_A^{0j}(t,0,\boldsymbol{p})=-p^j t\frac{\hat{f}_P(\boldsymbol{p})\hat{G}_P(\boldsymbol{p})}{2\hat{E}_P(\boldsymbol{p})}e^{-t\hat{E}_P(\boldsymbol{p})}+\cdots, \qquad (B15)$$

which in the rest frame of the meson becomes

$$C_A^{0j}(t,0,\boldsymbol{0})=0+\cdots \qquad (B16)$$

As explained in Ref. [7], Eq. (B11) allows one to subtract the point-like contribution from the diagonal spatial components C_A^{ii} nonperturbatively to all orders in the lattice spacing a. From Eqs. (B14) and (B15), we see that instead in the limit $k\to0$ the contribution from the $P(\boldsymbol{p}-\boldsymbol{k})+\gamma$ state exactly cancels the signal. Hence, for such components, it is not possible to extract, in the exact limit $k=0$, the physical matrix element from the Euclidean three-point function. We remark that in our analysis we have not used the purely temporal component C_A^{00}, which would make it difficult to identify the plateaux due to the presence of a large contribution from the excited state $P(\boldsymbol{p}-\boldsymbol{k})+\gamma$, at small values of k.

Finally, it is worth noting the peculiar behavior in t of the purely temporal component of the lattice three-point function, $C_A^{00}(t,0,\boldsymbol{p})$. From Eq. (B12) it can be seen that $C_A^{00}(t,0,\boldsymbol{p})$ exhibits a time behavior of type $te^{-t\hat{E}_P(\boldsymbol{p})}$, which is a manifestation of the singular behavior of the correlation function at large distances, and which gives rise to a double pole in momentum space. In our simulation we found numerical evidence for the presence of such a behavior. This is shown in Fig. 16, where we compare our numerical data for $H_{L,A}^{00}(t,0,\boldsymbol{0})$, defined in Eq. (28), with the prediction of Eq. (B12).
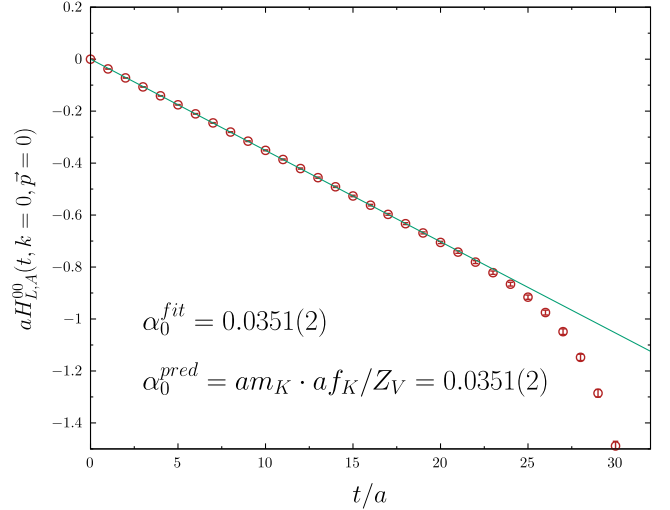

FIG. 16. Determination of the 00 component of the hadronic tensor, from the lattice three-point correlation function at $k=0$. The green line is the result of a linear fit in time $aH_{L,A}^{00}(t,0,\boldsymbol{0})=-\alpha_0^{fit}t$, where α_0^{fit} is a fit parameter, and which is compared with the predicted value, α_0^{pred}, derived from Eq. (B12). The fit was performed in the interval $t=(4,21)$, away from the center of the lattice where backward-propagating contributions to the correlation function become significant.

APPENDIX C: CORRELATION MATRICES FOR THE FORM FACTOR FIT PARAMETERS

In Tables VIII and IX we report the correlation matrices for the form factor fit parameters, the values of which are presented in Table II. Since we adopted two different fitting *Ansätze*, given in Eqs. (46) and (47), we have two different 12×12 matrices. Indeed, there are four form factors, each one described by a function defined through three parameters, and so there are 12 different parameters for each *Ansatz*. Given two different parameters A and B, the correlation between them has been computed according to

$$\rho_{A,B}=\frac{\sum_i(A_i-\mu_A)(B_i-\mu_B)}{\sqrt{\sum_i(A_i-\mu_A)^2}\sqrt{\sum_i(B_i-\mu_B)^2}}, \qquad \mu_A=\frac{1}{N}\sum_i A_i,$$

$$\mu_B=\frac{1}{N}\sum_i B_i, \qquad (C1)$$

where A_i and B_i are the jackknife samples for two parameters and the sum runs over all the jackknifes.

We remark that the lattice analysis is affected by systematic uncertainties due to the missing chiral, continuum and infinite-volume extrapolations that will be studied in future works. As a consequence, all the present numerical results should be taken as qualitative ones and as an indication of the feasibility of the method, and not as physical results.

TABLE VIII. Correlation matrix for the fit parameters corresponding to the polynomial fit described in Eq. (46).

Polynomial fit	a_{0,H_1}	a_{k,H_1}	a_{q,H_1}	a_{0,H_2}	a_{k,H_2}	a_{q,H_2}	a_{0,F_A}	a_{k,F_A}	a_{q,F_A}	a_{0,F_V}	a_{k,F_V}	a_{q,F_V}
a_{0,H_1}	1	−0.49	0.33	0.89	−0.58	−0.016	0.34	−0.79	−0.64	0.44	−0.18	0.18
a_{k,H_1}	−0.49	1	−0.40	−0.38	0.31	0.10	−0.65	0.60	0.19	0.076	−0.052	0.14
a_{q,H_1}	0.33	−0.40	1	0.30	−0.51	−0.66	−0.017	−0.081	−0.24	0.40	−0.56	0.27
a_{0,H_2}	0.89	−0.38	0.30	1	−0.76	−0.083	0.37	−0.75	−0.61	0.37	−0.28	0.27
a_{k,H_2}	−0.58	0.31	−0.51	−0.76	1	0.33	−0.31	0.54	0.45	−0.48	0.34	−0.44
a_{q,H_2}	−0.016	0.10	−0.66	−0.083	0.33	1	0.18	−0.24	−0.31	−0.46	0.11	−0.37
a_{0,F_A}	0.34	−0.65	−0.017	0.37	−0.31	0.18	1	−0.74	−0.10	−0.24	0.17	−0.20
a_{k,F_A}	−0.79	0.60	−0.081	−0.75	0.54	−0.24	−0.74	1	0.48	−0.16	0.00048	−0.14
a_{q,F_A}	−0.64	0.19	−0.24	−0.61	0.45	−0.31	−0.10	0.48	1	−0.17	0.53	0.14
a_{0,F_V}	0.44	0.076	0.40	0.37	−0.48	−0.46	−0.24	−0.16	−0.17	1	−0.22	0.76
a_{k,F_V}	−0.18	−0.052	−0.56	−0.28	0.34	0.11	0.17	0.00048	0.53	−0.22	1	−0.20
a_{q,F_V}	0.18	0.14	0.27	0.27	−0.44	−0.37	−0.20	−0.14	0.14	0.76	−0.20	1

TABLE IX. Correlation matrix for the fit parameters corresponding to the polynomial fit described in Eq. (47).

Pole fit	A_{H_1}	R_{k,H_1}	R_{q,H_1}	A_{H_2}	R_{k,H_2}	R_{q,H_2}	A_{F_A}	R_{k,F_A}	R_{q,F_A}	A_{F_V}	R_{k,F_V}	R_{q,F_V}
A_{H_1}	1	−0.57	0.13	0.87	−0.69	0.25	−0.48	−0.63	−0.58	0.49	−0.26	0.20
R_{k,H_1}	−0.57	1	−0.45	−0.48	0.46	−0.075	−0.10	0.70	0.25	−0.094	0.0058	0.034
R_{q,H_1}	0.13	−0.45	1	−0.0030	−0.37	−0.58	−0.019	0.038	−0.15	0.17	−0.51	0.24
A_{H_2}	0.87	−0.48	−0.0030	1	−0.62	0.34	−0.36	−0.61	−0.52	0.21	−0.25	0.12
R_{k,H_2}	−0.69	0.46	−0.37	−0.62	1	−0.053	0.25	0.49	0.48	−0.41	0.42	−0.45
R_{q,H_2}	0.25	−0.075	−0.58	0.34	−0.053	1	−0.096	−0.45	−0.47	−0.31	0.042	−0.27
A_{F_A}	−0.48	−0.10	−0.019	−0.36	0.25	−0.096	1	−0.15	0.43	−0.52	0.37	−0.40
R_{k,F_A}	−0.63	0.70	0.038	−0.61	0.49	−0.45	−0.15	1	0.25	−0.069	−0.089	−0.080
R_{q,F_A}	−0.58	0.25	−0.15	−0.52	0.48	−0.47	0.43	0.25	1	−0.049	0.57	0.17
A_{F_V}	0.49	−0.094	0.17	0.21	−0.41	−0.31	−0.52	−0.069	−0.049	1	−0.17	0.67
R_{k,F_V}	−0.26	0.0058	−0.51	−0.25	0.42	0.042	0.37	−0.089	0.57	−0.17	1	−0.37
R_{q,F_V}	0.20	0.034	0.24	0.12	−0.45	−0.27	−0.40	−0.080	0.17	0.67	−0.37	1

[1] R. Aaij *et al.* (LHCb Collaboration), Nat. Phys. **18**, 277 (2022).
[2] A. Crivellin and M. Hoferichter, Science **374**, 1051 (2021).
[3] N. Carrasco, A. Deuzeman, P. Dimopoulos, R. Frezzotti, V. Giménez, G. Herdoiza, P. Lami, V. Lubicz, D. Palao, E. Picca *et al.*, Nucl. Phys. **B887**, 19 (2014).
[4] V. Lubicz, G. Martinelli, C. T. Sachrajda, F. Sanfilippo, S. Simula, and N. Tantalo, Phys. Rev. D **95**, 034504 (2017).
[5] D. Giusti, V. Lubicz, G. Martinelli, C. T. Sachrajda, F. Sanfilippo, S. Simula, N. Tantalo, and C. Tarantino, Phys. Rev. Lett. **120**, 072001 (2018).
[6] M. Di Carlo, D. Giusti, V. Lubicz, G. Martinelli, C. T. Sachrajda, F. Sanfilippo, S. Simula, and N. Tantalo, Phys. Rev. D **100**, 034514 (2019).
[7] A. Desiderio, R. Frezzotti, M. Garofalo, D. Giusti, M. Hansen, V. Lubicz, G. Martinelli, C. T. Sachrajda, F. Sanfilippo, S. Simula, and N. Tantalo, Phys. Rev. D **103**, 014502 (2021).
[8] R. Frezzotti, M. Garofalo, V. Lubicz, G. Martinelli, C. T. Sachrajda, F. Sanfilippo, S. Simula, and N. Tantalo, Phys. Rev. D **103**, 053005 (2021).
[9] P. Zyla *et al.* (Particle Data Group), Prog. Theor. Exp. Phys. **2020**, 083C01 (2020).
[10] A. A. Poblaguev, R. Appel, G. S. Atoyan, B. Bassalleck, D. R. Bergman, N. Cheung, S. Dhawan, H. Do, J. Egger, S. Eilerts *et al.*, Phys. Rev. Lett. **89**, 061803 (2002).
[11] H. Ma, R. Appel, G. S. Atoyan, B. Bassalleck, D. R. Bergman, N. Cheung, S. Dhawan, H. Do, J. Egger, S. Eilerts *et al.*, Phys. Rev. D **73**, 037101 (2006).
[12] R. Aaij, C. A. Beteta, B. Adeva, M. Adinolfi, C. A. Aidala, Z. Ajaltouni, S. Akar, P. Albicocco, J. Albrecht *et al.*, Eur. Phys. J. C **79**, 675 (2019).

[13] X.-Y. Tuo, X. Feng, L.-C. Jin, and T. Wang, Phys. Rev. D **105**, 054518 (2022).

[14] L. Lellouch and M. Luscher, Commun. Math. Phys. **219**, 31 (2001).

[15] C. h. Kim, C. T. Sachrajda, and S. R. Sharpe, Nucl. Phys. **B727**, 218 (2005).

[16] R. A. Briceño, Z. Davoudi, M. T. Hansen, M. R. Schindler, and A. Baroni, Phys. Rev. D **101**, 014509 (2020).

[17] J. Bijnens, G. Colangelo, G. Ecker, and J. Gasser, arXiv:hep-ph/9411311.

[18] A. Danilina, N. Nikitin, and K. Toms, Phys. Rev. D **101**, 096007 (2020).

[19] N. Carrasco, V. Lubicz, G. Martinelli, C. Sachrajda, N. Tantalo, C. Tarantino, and M. Testa, Phys. Rev. D **91**, 074506 (2015).

[20] L. Maiani and M. Testa, Phys. Lett. B **245**, 585 (1990).

[21] R. Frezzotti, P. A. Grassi, S. Sint, and P. Weisz (Alpha Collaboration), J. High Energy Phys. 08 (2001) 058.

[22] R. Frezzotti and G. Rossi, J. High Energy Phys. 08 (2004) 007.

[23] G. M. de Divitiis, R. Frezzotti, V. Lubicz, G. Martinelli, R. Petronzio, G. C. Rossi, F. Sanfilippo, S. Simula, and N. Tantalo, Phys. Rev. D **87**, 114505 (2013).

[24] G. de Divitiis, R. Petronzio, and N. Tantalo, Phys. Lett. B **595**, 408 (2004).

[25] J. M. Flynn, A. Jüttner, C. Sachrajda, P. A. Boyle, J. M. Zanotti, and UKQCD Collaboration, J. High Energy Phys. 05 (2007) 016.

[26] C. T. Sachrajda and G. Villadoro, Phys. Lett. B **609**, 73 (2005).

[27] K. Jansen, A. Shindler, C. Urbach, and I. Wetzorke (XLF Collaboration), Phys. Lett. B **586**, 432 (2004).

[28] A. Shindler, Phys. Rep. **461**, 37 (2008).

[29] J. Bijnens and G. Ecker, Annu. Rev. Nucl. Part. Sci. **64**, 149 (2014).

[30] S. Krishna and H. S. Mani, Phys. Rev. D **5**, 678 (1972).

[31] V. Shtabovenko, R. Mertig, and F. Orellana, Comput. Phys. Commun. **256**, 107478 (2020).

[32] G. P. Lepage, J. Comput. Phys. **27**, 192 (1978).